AD-A275 745

DARPA/ONR Grant #N00014-91-J-1976

10th Quarterly Progress Report
(covering the period of 11/01/93 - 01/31/94)

**Project Title: Development of Ultra-Low Noise, High Performance
III-V Quantum Well Infrared Photodetectors (QWIPs)
for Focal Plane Array Staring Image Sensor Systems**

Submitted to

Max N. Yoder

Office of Naval Research
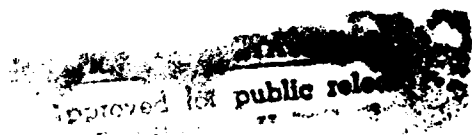Code 3140
800 North Quincy Street
Arlington, VA 22217-5000

DTIC
ELECTE
FEB 15 1994
E   D

Prepared by

Sheng S. Li
Professor

Dept. of Electrical Engineering
University of Florida
Gainesville, Florida 32611   DTIC QUALITY INSPECTED 2

Tel.(904)-392-4937
Fax(904)-392-8671
E-Mail: ShengLi@ENG.UFL.EDU

Approved for public release

February 6, 1994

94-05007

94 2 14 048

REPORT DOCUMENTATION PAGE

Public reporting burden for this collection of information is estimated to average 1 hour per response, including the time for reviewing instructions, searching existing data sources, gathering and maintaining the data needed, and completing and reviewing the collection of information. Send comments regarding this burden estimate or any other aspect of this collection of information, including suggestions for reducing this burden, to Washington Headquarters Services, Directorate for Information Operations and Reports, 1215 Jefferson Davis Highway, Suite 1204, Arlington, VA 22202-4302, and to the Office of Management and Budget, Paperwork Reduction Project (0704-0188), Washington, DC 20503

1. AGENCY USE ONLY (Leave blank)	2. REPORT DATE February 1, 94	3. REPORT TYPE AND DATES COVERED Quarterly progress report: 11/1/93 - 01/31/94.

4. TITLE AND SUBTITLE	5. FUNDING NUMBERS
Development of Ultra-Low Noise, High Sensitivity Planar Metal Grating Coupled III-V Quantum Well Infrared Detectors for Focal Plane Array Staring IR Sensor Systems	ONR G-N00014-91-J-1976

6. AUTHOR(S)

Sheng S. Li, Professor

7. PERFORMING ORGANIZATION NAME(S) AND ADDRESS(ES)	8. PERFORMING ORGANIZATION REPORT NUMBER
University of Florida Gainesville, FL 32611-6200	92122803

9. SPONSORING / MONITORING AGENCY NAME(S) AND ADDRESS(ES)	10. SPONSORING / MONITORING AGENCY REPORT NUMBER
US Navy, Office of Naval Research 800 North Quincy Street, Code 1512B:SM Arlington, VA 22217-5000	

11. SUPPLEMENTARY NOTES

12a. DISTRIBUTION / AVAILABILITY STATEMENT	12b. DISTRIBUTION CODE
Approved for public release, distribution unlimited.	

13. ABSTRACT (Maximum 200 words)

During this reporting period (11-01-93 to 01-31-94) we have continued to make significant progress towards the program goals. We have developed a new normal incidence p-type strained-layer InGaAs/InAlAs QWIP grown on InP by MBE. This PSL QWIP has achieved an ultra-low dark current and very high detectivity at 8.1 um and 77 K. The detector is under background limited performance (BLIP) for T<100 K, which is the highest BLIP temperature ever reported for a QWIP. A dark current density of 7×10^{-8} A/cm^2 and BLIP detectivity of 5.9×10^{10} Jones were obtained for this QWIP at 77 K. Other tasks perrformed during this period include: (i) Design, fabrication and characterization of a new two-color stacked BTM and BTC QWIP for 3-5 and 8-12 um IR detection, (ii) design and fabrication and characterization of a normal incidence p-type compressive strained -layer InGaAs/GaAs QWIP grown on GaAs, and (iii) theoretical and experimental studies of parameter optimization for an InGaAs BTM QWIP. Detailed results and accomplishments are described in this report.

14. SUBJECT TERMS		15. NUMBER OF PAGES
GaAs/GaAlAs Quantum well infrared photodetectors (QWIPs), p-type strained-layer InGaAs/GaAs QWIP, intersubband absorption, dark current, responsivity, detectivity, 2 color stack QWIP.		16. PRICE CODE

17. SECURITY CLASSIFICATION OF REPORT	18. SECURITY CLASSIFICATION OF THIS PAGE	19. SECURITY CLASSIFICATION OF ABSTRACT	20. LIMITATION OF ABSTRACT
Unclassified.			Unlimited

10th Quarterly Progress Report (11/1/93 - 01/31/94)

Project Title: Development of Ultra-Low Dark Current, High Performance III-V Quantum Well Infrared Photodetectors (QWIPs) for Focal Plane Arrays Staring Imaging Sensor Systems.

Program Manager: Max N. Yoder, Office of Naval Research, Code 3140, Arlington, VA.

Principal Investigator: Sheng S. Li, Professor, University of Florida, Gainesville, FL.

Project Objectives:

1. To develop ultra-low dark current and high detectivity planar metal grating coupled bound-to-miniband (BTM) transition III-V quantum well infrared photodetectors (QWIPs) for 8 to 14 μm focal plane arrays (FPAs) staring IR image sensor systems.

2. To develop novel III-V QWIPs with single, multicolor, broad- and narrow-spectral responses in the 8 to 14μm wavelength range. The material systems to be studied include n-type GaAs/AlGaAs, InGaAs/GaAs and AlAs/AlGaAs grown on GaAs, and InGaAs/InAlAs on InP; p-type strained-layer InGaAs/InAlAs on InP and InGaAs/GaAs on GaAs substrates.

3. To conduct theoretical and experimental studies of the planar 2-D metal grating coupled structures for normal incidence illumination on QWIPs. Different metal grating coupled structures using 2-D square and circular mesh metal gratings will be studied in order to achieve high coupling quantum efficiency under normal incident front side or back side illuminations.

4. To perform theoretical and experimental studies of dark current, noise figures, optical absorption, spectral responsivity and detectivity for all types of QWIPs to be developed under this program.

1

I. Introduction

During this reporting period (11-01-93 to 01-31-94) we have continued to make excellent progress towards the program goals. Specific tasks performed during this period include: (i) designed, fabricated, and characterized a new normal incidence p-type compressive strained-layer (SL) $In_{0.4}Ga_{0.6}As/GaAs$ QWIP formed on GaAs substrate, which simultaneously achieved the two-color detection at mid-wavelength infrared (MWIR) of 4 - 7 μ and long-wavelength infrared (LWIR) at 8 - 14 μ at T = 75 K, (ii) designed, fabricated, and characterized a new two-color enhanced bound-to-continuum band (EBTC) and bound-to-miniband (BTM) transition GaAs/GaAlAs QWIPs grown on GaAs substrate, and (iii) performed theoretical and experimental studies on the effects of grating period, quantum well doping density and barrier height on the performance of a grating coupled InGaAs BTM QWIP with and without waveguide structure. A list of accomplishments and publications are given in Section II. The technical results are presented in Section III.

II. Research Accomplishments and Publications

Research accomplishments and publications supported by this ARPA/ONR grant are summarized as follows:

2.1 Research Accomplishments:

1. A new normal incidence p-type strained (PSL) InGaAs/InAlAs QWIP with peak response wavelength at $\lambda_p = 8.1$ μm and operating under background limited performance (BLIP) condition at 77 K has been developed for the first time. This detector is under BLIP for T $\leq$ 100 K, which is the highest BLIP temperature ever reported for a QWIP. The BLIP detectivity for this QWIP at peak wavelength $\lambda_p = 8.1$ μm was found to be 5.9×10^{10} $cm - Hz^{1/2}/W$, at $V_b = 2$ V and T = 77 K. The extremely low dark current density (7×10^{-8} A/cm^2) observed in this QWIP at 77 K offers an excellent opportunity to fabricate high performance focal plane arrays using PSL-QWIPs for 77 K operation.

2. Design and growth of a new normal incidence p-type compressive strained-layer InGaAs/GaAs QWIP on SI GaAs substrate have been made. Device fabrication and characterization for this new QWIP have been carried out and the results are presented in Section 3.1.

3. Design, growth, fabrication, and characterization of a new two-color enhanced bound-to-continuum band (EBTC) and bound-to-miniband (BTM) transition GaAs/GaAlAs QWIPs

2

grown on GaAs substrate have been carried out and the results are described in Section 3.2.

4. Conduct theoretical and experimental studies on the effects of grating period, quantum well doping density and barrier height on the performance of a grating coupled InGaAs BTM QWIP with and without waveguide structure, and the results are depicted in Section 3.3.

5. Since the beginning of this project, one Ph.D. and three M.S. students have completed their degree working on the QWIP project sponsored by the ARPA/ONR grant. Two more Ph.D. students are in their final stage of research and are expected to graduate by Summer semester, 1994. An AASERT sponsored Ph.D. student has started in July, 1993 working on the new high performance normal incident p-type strained-layer InGaAs/InAlAs QWIPs for focal plane arrays applications.

6. Dr.Li presented an **invited talk** on the Grating Coupled and Normal Incidence III-V QWIPs at the *NATO Advanced Research Workshop on Intersubband Transition Physics and Devices*, Whistler, Canada, Sept.7-10, 1993.

7. Dr.Li presented an **invited talk** on Grating Coupled III-V QWIPs for Mid- and Long-Wavelength Infrared (LWIR) Detection,at the *First Int. Symposium on Long Wavlength Infrared Detectors and Arrays*, Electrochemical Society Meeting, New Orlean, October 10-13, 1993.

8. Dr. Li has completed a book chapter (chapter 4, 80 pages) on **Metal Grating Coupled Bound-to-Miniband (BTM) Transition Quantum Well Infrared Photodetectors** for a monograph on *Long Wavelength Quantum Well Infrared Photodetectors* edited by Dr. Manasreh and to be published by Artech House in 1994.

2.2. Refereed Journal Papers:

1. L. S. Yu andS. S. Li,"A Low Dark Current, High Detectivity Grating Coupled AlGaAs/GaAs Mulitple Quantum Well IR Detector Using Bound-to-Miniband Transition for 10 μm Detection,"Appl. Phys. Letts., 59 (11), p.1332, Sept.9, 1991.

2. L. S. Yu,S. S. Li, and Pin Ho "Largely Enhanced Bound-to-Miniband Absorption in an InGaAs Multiple Quantum Well with a Short-Period Superlattice InAlAs/InGaAs Barrier " Applied Phys. Letts., 59 (21), p.2712, Nov. 18, 1991.

3. L. S. Yu, Y. H. Wang, S. S. Li and Pin Ho, "A Low Dark Current Step-Bound-to-Miniband Transition InGaAs/GaAs/AlGaAs Multiquantum Well Infrared Detector," Appl. Phys. Letts., 60(8), p.992, Feb.24, 1992.

4. L. S. Yu, S. S. Li, and P. Ho, "A Normal Incident Type-II Quantum Well Infrared Detector Using an Indirect AlAs/Al$_{0.5}$Ga$_{0.5}$As System Grown on [110] GaAs," Electronics Letts., 28(15) p.1468, July,16, 1992.

5. L. S. Yu, S. S. Li, Y. H. Wang, and Y. C. Kao, "A Study of Coupling Efficiency versus Grating Periodicity in A Normal Incident Grating-Coupled GaAs/AlGaAs Quantum Well Infrared Detector," J. Appl. Phys., 72(6), pp.2105, Sept. 15, 1992.

6. Y. H. Wang, S, S. Li, and P. Ho, "A Photovoltaic and Photoconductive Dual Mode Operation GaAs/AlGaAs Quantum Well Infrared Detector for Two Band Detection," Appl.Phys. Lett., 62(1), pp.93-95, Jan. 4 1993.

7. Y. H. Wang, S. S. Li, and P. Ho, "A Voltage-Tunable Dual Mode Operation InAlAs/InGaAs Bound-to-Miniband Transition QWIP for Narrow and Broad Band Detection at 10 μm," Appl. Phys. Lett., 62(6), pp.621-624, Feb. 8 , 1993.

8. P. Ho, P. A. Martin, L. S. Yu, and S. S. Li, "Growth of GaAs and AlGaAs on Misoriented (110) GaAs and a Normal Incidnece Type-II Quantum Well Infrared Detector," J. Vacuum Science and Technology B,11(3), pp.935-944, May/June, 1993.

9. S. S. Li, M. Y. Chuang and L. S. Yu, "Current Conduction Mechanisms in Bound-to-Miniband Transition III-V Quantum Well Infrared Photodetectors," *J. Semiconductor Science and Technology*, vol.8, pp.406-411, 1993.

10. Y. H. Wang, S. S. Li, P. Ho, and M. O. Manasreh, "A Normal Incidence Type-II Quantum Well Infrared Photodetector Using An Indirect AlAs/AlGaAs System Grown on [110] GaAs for the Mid- and Long-Wavelength Multicolor Detection," J. Appl. Phys., vol.74(2), pp.1382-87, July 15, 1993.

11. Y. C. Wang and S. S. Li, "A Numerical Analysis of Double Periodic Reflection Metal Grating Coupler for Multiquantum Well Infrared Photodetectors," J. Appl.Phys.,vol.74(4), pp.2192-96, August 15, 1993.

12. Y. C. Wang and S. S. Li, "Design of A Two-Dimensional Square Mesh Metal Grating Coupler for GaAs/AlGaAs Quantum Well Infrared Photodetectors," J. Appl.Phys., vol.75(1), Jan.1, pp.582-587, 1994.

13. Y. H. Wang, S. S. Li, J. Chu, and P. Ho, "An Ultra-low Dark Current Normal Incidence P-type Strained Layer InGaAs/InAlAs QWIP with Background Limited Performance at 77 K," Appl. Phys. Lett., to be appeared in February 7 issue, 1994.

2.3. Workshop and Conference Presentations

1. L. S. Yu, S. S. Li, and Pin Ho, " Largely Enhanced Intra-subband Absorption in a Wide InAlAS/InGaAs Quantum Well with a Short-Period Superlattice Barrier Structure,' presented at the *SPIE's Symposium on Quantum Wells and Superlattices*, Somerset, NJ, 23-27 March,1992. Paper published in the SPIE Conference Proceeding.

2. S. S. Li and L. S. Yu, "Grating Coupled Bound-to-Miniband Transition III-V Quantum Well Infrared Detectors," **Invited Talk**, presented at *the Innovative Long Wavelength Infrared Photodetector Workshop*, Jet Propulsion Lab., Pasadena, CA, April 7-9, 1992.

3. L. S. Yu and S. S. Li, "A Normal Incident Type-II Quantum Well Infrared Detector Using an Indirect AlAs/Al$_{0.5}$Ga$_{0.5}$As System Grown on [110] GaAs, presented at *the Innovative Long Wavelength Infrared Photodetector Workshop*, Jet Propulsion Lab., Pasadena, CA, April 7-9, 1992.

4. L. S. Yu, S. S. Li, Y. H. Wang, and P. Ho, " Grating Coupled III-V Quantum Well Infrared Detectors Using Bound-to-Miniband Transition," presented at *the SPIE Conference on Infrared Detectors and Focal Plane Arrays at OE/Aerospace Sensing 92*," Orlando, FL, April 20-24, 1992. Full paper published in the SPIE conference proceeding.

5. S. S. Li, "Grating Coupled Bound-to-Miniband Transition III-V Multiquantum Well Infrared Photodetectors," presented at the DARPA IR Detector Workshop, Washington D.C., June 12, 1992.

6. S. S. Li, M. Y. Chuang and L. S. Yu, "Current Conduction Mechanisms in Bound-to-Miniband Transition III-V Quantum Well Infrared Photodetectors," presented at the *International Conference on Narrow Gap Semiconductors*, University of Southampton, Southampton, UK, July 19-23, 1992.

7. P. Ho, P. A. Martin, L. S. Yu, and S. S. Li,"Growth of GaAs and AlGaAs on Misoriented (110) GaAs and a Normal Incidnece Type-II Quantum Well Infrared Detector," presented at the *12th North American Conference on Molecular Beam Epitaxy*," Oct.12-14, 1992.

8. S. S. Li,"Novel Grating Coupled Miniband Transport III-V Multiquantum Well Infrared Photodetectors for Focal Plane Array Applications," presented at the DARPA IR Detector Workshop, Washington D.C., Dec 11, 1992.

9. S. S. Li, Y. H. Wang, M. Y. Chuang, P. Ho,"Photoconductive and Photovoltaic Dual-Mode Operation III-V Quantum Well Infrared Photodetectors for 2 - 14 μm Detection," presented at the Materials Research Society (MRS), Symposium C2 on **Infrared Detectors**, San Francisco, April 12-16, 1993.

10. D. Wang, Y. H. Wang, G. Bosman and S. S. Li,"Noise Characterization of Novel Quantum Well Infrared Photodetectors," **Invited Talk** presented at the *12th Int. Conf. on Noise in Physical Systems and 1/f Fluctuations - The High Technologies Conference*, St. Louis, MO, August 16-20, 1993.

11. S. S. Li,"Some Novel High Performance III-V Quantum Well Infrared Photodetectors for Focal Plane Array Image Sensor Applications," **Invited Talk** presented at *the NATO Advanced Research Workshop on Intersubband Transition Physics and Devices*, Whistler, Canada, September 7 - 10, 1993.

12. S. S. Li,"Grating Coupled III-V Quantum Well Infrared Photodetectors for Mid-Wavelength and Long-Wavelength Infrared Detection," **Invited Talk** presented at *the First International Symposium on Long Wavelength Infrared Photodetectors* in conjunction with the Fall Electrochemical Society (ECS) Meeting in New Orlean, LA, October 10 -15, 1993.

13. S. S. Li, Y. H. Wang, J. Chu, and P. Ho,"A Normal Incidence P-Type Strained-Layer In-GaAs/InAlAs Quantum Well Infrared Photodetector with Background Limited Performance at 77 K," 1994 *SPIE Conference on Infrared Detectors and Focal Plane Arrays III*, Orlando, FL, April 4-6, 1994.

2.4 Interactions with Government and Industrial Laboratories

1. Continued to collaborate with Dr. Pin Ho of General Electric Co.,in Syracuse, NY, on the growth of III-V QWIP's structures by using the MBE technique.

6

2. Contiuned to interact and exchange technical information on QWIP results with Dr. M. Tidrow of U.S. Army Electronics Tech. & Devices Laboratory, EPSD, Fort Monmouth, NJ.

3. Dr. Li was invited to give a seminar at the Electronics Technology Laboratory, WPAFB, Ohio, on *The bound-to-miniband transition III-V QWIPs* on August 21, 92, and discussed with Dr.Omar Manasreh and his colleagues in the Electronics Technology Laboratory at the WPAFB. Dr. Manasreh had performed optical absorption measurements on Dr. Li's QWIP samples, while Dr. Li has fabricated and characterized some QWIP samples provided by Dr. Manasreh.

4. Dr. Li was invited by the American Engineering Education Association (AEEA) to serve on a review panel for Naval Postdoctoral Fellowship program in Washington D.C. August 7, 92, to review a dozen of proposals submitted by various applicants.

5. Mr. Tom Briere of InfraMetrics has contacted Dr. Li, expressing his interest in using our QWIPs in the infrared imaging sensor applications. Dr. Li has sent a copy of his most recent ARPA quarterly progress report to Mr. Briere. Dr. Li will keep in touch with InfraMetrics on our new development in QWIP arrays.

6. Dr. Li has collaborated with Drs. Bill Beck and John Little of Martin Marietta Lab. (MML), in Baltimore, Maryland on p-type QWIP research. Dr. Li has sent a PSL-InGaAs/InAlAs QWIP sample to Dr. Beck for evaluation and for possible fabrication of focal plane arrays at MML.

7. Drs.Jan Andersson and Len Lundqvist (both working on grating coupled QWIP arrays) visited Dr. LI's Lab. on October 15, 1993, and presented a seminar on grating design for grating coupled GaAs QWIPs in our Department.

8. Dr. Li has been invited by Electrochemcial Society (ECS) to serve as co-organizer for the *2nd. International Symposium on 2-20 µm Wavelength Infrared Detectors and Arrays: Physics and Applications* to be held in Miami Beach, FL., October10-15, 1994. A call for papers has been sent out to MTC and IR community.

9. The p-type strained-layer InGaAs/InAlAs QWIP developed recently in our Lab. has received considerable interest in the QWIP community. We have received many requests from industry, university, and government Labs. for the preprints of the PSL-QWIP paper presented at *the 1993 NATO Advanced Research Workshop on Intersubband Transition Physics and Devices*

and *the First International Symposium on Long Wavelength Infrared Detectors and Arrays-ECS 93'.*

10. Dr. Anjali Singh of the Passive Sensors Branch at Kirkland AFB, NM, has contacted Dr. Li concerning our QWIP research. She has indicated that her Quantum Well Working Group are very interested in our work miniband transport QWIPs and would like to establish research collaboration on QWIPs. Dr. Li has sent his most recent publications and reports to her for information and reference.

III. Technical Results

3.1 A P-type Compressive Strained-Layer InGaAs/GaAs QWIP for MWIR and LWIR Detection

Summary: A new normal incidence p-type compressive strained-layer $In_{0.4}Ga_{0.6}As$/GaAs quantum well infrared photodetector (PSL-QWIP) grown on (100) semi-insulating GaAs substrate by MBE technique for 4-7 μm mid-wavelength infrared (MWIR) and 8-14 μm long wavelength infrared (LWIR) two-color detection has been demonstrated for the first time. This PSL-QWIP shows a broadband double-peak response at MWIR and LWIR detection bands by utilizing the resonant transport coupling mechanism between the heavy-hole type-I states and the light-hole type-II states. Using the compressive strain in the InGaAs quantum well, normal incident absorption was greatly enhanced by reducing the heavy-hole effective mass (by a factor of 3) and increasing the density of states of the off-zone center. Maximum responsivities of 93 mA/W and 30 mA/W at peak wavelengths of λ_{p1} = 8.9 μm and λ_{p3} = 5.5 μm, respectively, were obtained at V_b = 1.6 V and T = 75 K. This PSL-QWIP shows a background limited performance (BLIP) at $V_b \leq 0.3$ V and T = 75 K for the 8-14 μm LWIR detection band.

3.1.1 Introduction

Quantum well infrared photodetectors (QWIPs) using n-type GaAs/AlGaAs and InGaAs/InAlAs material systems for the 3 - 5 μm MWIR and 8 - 14 μm LWIR atmospheric transmission windows have been extensively studied in recent years[1-6]. With low electron effective mass and high electron mobility, the n-type GaAs and InGaAs QWIPs offer excellent IR detection properties. However, quantum mechanical selection rule for the intersubband transition requires that the radiation electric field has a component perpendicular to the quantum well plane in order to induce intersubband absorption in the quantum wells. As a result, for n-type QWIPs, it is necessary to use planar metal

8

or dielectric grating structures for coupling the normal incident IR radiation in an absorbable angle into the quantum well[3-5].

P-type QWIPs using valence intersubband transitions have been demonstrated in the lattice-matched GaAs/AlGaAs and InGaAs/InAlAs material systems[7-9]. Due to band mixing between the light-hole and heavy-hole states, the normal incident illumination is allowed for inducing intersubband transition in p-type QWIPs. In general, the intersubband transitions under normal incident radiation in p-type quantum wells are induced by the linear combination of p-like valence-band Bloch states which provides a nonzero coupling between this component and the normal radiation field. The strong mixing between the light- and heavy-hole states at $\mathbf{k} \neq 0$ greatly enhances the normal incidence intersubband absorption. However, in the unstrained lattice-matched quantum well systems, this intersubband transition occurs between the heavy-hole ground state and the upper excited states. Due to a large heavy-hole effective mass, weak absorption and low responsivity are expected in the unstrained p-QWIPs. Recently, we reported the first normal incident p-type strained-layer InGaAs/InAlAs QWIP grown on the InP substrate[10], in which a biaxial tensile strain was used in the InGaAs quantum wells. It is shown that using a strained-layer structure in a p-type QWIP can greatly increase its responsivity and BLIP temperature, and hence offers more flexibilities in QWIP fabrication. In this section we report a new normal incidence p-type compressive strained-layer (PSL) $In_{0.4}Ga_{0.6}As$/GaAs QWIP grown on semi-insulating (SI) GaAs substrate by the MBE technique. In this QWIP structure, electrons and heavy-holes are confined in a type-I quantum well configuration, while electrons and light-holes are confined in a type-II quantum well configuration. By carefully choosing the strength of compressive strain, quantum well growth direction and layer thickness, the continuum states of heavy-holes can be resonantly lined up with the continuum states of light-holes. As a result, a large photocurrent gain can be expected in such a QWIP structure.

3.1.2 Theory

In general, strain can greatly affect the energy band structure and induce splitting between the heavy-hole and light-hole states in the valence band zone-center, which is degenerated in the unstrained case. In the $In_{0.4}Ga_{0.6}As$/GaAs QWIP grown on the SI GaAs substrate, a biaxial compressive strain is introduced in the InGaAs quantum well layers while no strain is present in the GaAs barrier layers and substrate. The strain pushes the heavy-hole states upward and pulls the light-hole states downward in the InGaAs well region. The light- and heavy-hole bands are

splitted in the InGaAs well region and degenerated in the GaAs barrier region at the BZ center (i.e. $k = 0$).

In order to fully describe the optical and electronic properties (such as energy gap, subband energy level splitting, intersubband transitions etc.,) for the compressively strained InGaAs layers, we should use the multiband effective-mass k.p model under perturbation approximation, in which the interactions (i.e., mixing and coupling) among conduction (C), heavy-hole (HH), light-hole (LH), and spin-orbit (SO) bands are taken into consideration and the 8×8k.p Hamiltonian and momentum matrix are obtained. In this model, a set of wave functions of $S_{1/2}$, ($|1/2, \pm 1/2 >_c$), $P_{3/2}$, ($|3/2, \pm 3/2; \pm 1/2 >$), and $P_{1/2}$, ($|1/2, \pm 1/2 >$) are used as the unperturbed and unstrained basis in the $|J, m_J >$ representation[11]. $m_J = \pm 1/2$ represent light-particle states (either electron or LH), while $m_J = \pm 3/2$ denote the heavy-particle states (HH). Since a larger conduction bandgap exists in the InGaAs layers than the matrix elements of k.p between the conduction band and valence band states, a reduced 6×6 k.p Hamiltonian can be approximated in depicting the properties of InGaAs layers by ignoring the coupling from the conduction band S-like states. The wave functions at the zone center (i.e. $k = 0$) under the compressive strain are given by[12],

$$|3/2, \pm 3/2 > \qquad\qquad \text{HH states}$$
$$\alpha|3/2, \pm 1/2 > +\beta|1/2, \pm 1/2 > \quad \text{LH states}$$
$$-\beta|3/2, \pm 1/2 > +\alpha|1/2, \pm 1/2 > \quad \text{SO states}$$

where α and β arc constants depending on the strain parameters. It is seen that the heavy-hole states $|3/2, \pm 3/2 >$ are still decoupled with other valence states even under the compressive strain, while light-hole states and spin-orbit split-off states are coupled, at the BZ center. However, HH, LH, and SO states are mixed[13] if $k \neq 0$. This kind of mixtures (between the states with different m_J's) is due to boundary conditions across the interface of the quantum well layers. From k.p matrix, the interaction between the states are proportional to the transverse component of the wave vector (i.e. $k_{x,y}$), so that HH-states are decoupled when $k_{x,y} = 0$. Note that $k_{x,y}$ is conserved across the interfaces since interface potential depends only on z, the quantum well growth direction. The band mixing can be significant if the Γ-bandgap is small (in our case, InGaAs has very small direct energy bandgap) and if LH- and SO-bands involved in the transition have a large k_z[13].

From the elasticity theory[14], the biaxial strain can be divided into two independent components: one is isotropic or hydrostatic component and the other is anisotropic or shear uniaxial component. The strain-induced energy shifts due to the hydrostatic potential (ΔE_H) and the shear

uniaxial strain (ΔE_U), respectively, can be approximated by[15]

$$\Delta E_H = 2V_c \frac{C_{11} - C_{12}}{C_{11}} \delta_o \tag{1}$$

$$\Delta E_U = V_s \frac{C_{11} + 2C_{12}}{C_{11}} \delta_o \tag{2}$$

where δ_o (a_s - $a_{1,2}$)/$a_{1,2}$) is the lattice mismatch with respect to the substrate lattice constant a_s. V_c and V_s are the conduction band deformation potential and shear deformation potential, respectively. C_{ij} are the elastic constants.

The energy bandgaps for the heavy-hole, light-hole, and spin-orbit states are given by[17]

$$E_{HH} = E_o + \Delta E_H - \Delta E_U \tag{3}$$

$$E_{LH} = E_o + \Delta E_H + \Delta E_U - \frac{(\Delta E_U)^2}{2\Delta_o} + \cdots \tag{4}$$

$$E_{SO} = E_o + \Delta_o + \frac{(\Delta E_U)^2}{2\Delta_o} + \cdots \tag{5}$$

where E_o is the unstrained bandgap and Δ_o is the spin-orbit splitting. From the above equations, it can be shown that both the heavy-hole and light-hole states are shifted as a result of the biaxial strain and spin-orbit splitting energy.

3.1.3. Design of A PSL-InGaAs QWIP

In this section we describe a new normal incidence p-type compressive strained-layer (PSL) $In_{0.4}Ga_{0.6}As$/GaAs QWIP grown on the SI GaAs substrate by using MBE technique. This PSL-QWIP structure consists of 20 periods of 4-nm Be-doped $In_{0.4}Ga_{0.6}As$ quantum well with a dopant density of 4×10^{18} cm^{-3} separated by s 35-nm GaAs undoped barrier layer. A 0.3 μm cap layer and a 0.7 μm buffer layer of Be-doped GaAs with a dopant density of 5×10^{18} cm^{-3} were grown for the QWIP's top and bottom ohmic contacts. The contact and barrier layers are lattice-matched to the SI GaAs substrate, and the $In_{0.4}Ga_{0.6}As$ quantum well layers are undergone biaxial compression with a lattice mismatch of about 2.8% between the well and the barrier layers. The ground subband energy levels confined in the quantum wells are the highly populated heavy-hole states E_{HH1}. The mobility of the heavy-hole is enhanced by the compressive strain created in the InGaAs quantum well layers due to a reduction of the heavy-hole effective mass[16] (i.e.by a factor 3). In this InGaAs/GaAs strained-layer QWIP, the heavy-hole state is in type-I band alignment configuration, while the light-hole state is in type-II band alignment configuration. In addition, a binary GaAs barrier layer is employed so that a superior current transport is expected to that of a ternary barrier layers. It should be noted that unlike other types of QWIPs the heavily doped contact layers of this

11

PSL-QWIP are made using the large-bandgap GaAs. A large tunneling current from the triangle barrier potential near ohmic contact region may be the dominant factor. In order to reduce this dark current component, a thick (550 $\mathring{A}$) undoped GaAs barrier layer is grown next to the top and bottom contact layers.

Figure 3.1(a) and (b) show the energy band diagram and subband energy states for this PSL-QWIP. The intersubband transitions for this PSL-QWIP occurs from the highly populated ground heavy-hole state (E_{HH1}) to the upper heavy-hole continuum states (E_{HH3} and E_{HH4}) for the 8.8 μm long-wavelength detection and 5 μm mid-wavelength detection, respectively. As shown in the Fig.3.1, the combination of type-I (for heavy-hole) and type-II (for light-hole) energy band configurations has three main ingradients to improve the performance of this QWIP. First, the mobility of the heavy-holes confined in the ground states (i.e. HH1) of type-I configuration is enhanced by the internal biaxial compressive strain effect, for which a larger normal absorption should be achieved. Second, the heavy-hole excited continuum states (i.e. HH3) are resonance with the GaAs barrier which can maximize the absorption oscillator strength. Finally, the heavy-hole excited continuum states are resonantly lined up with the light-hole states, which may give rise to a strong quantum state coupling effect. It is the resonant line-up effect that makes the conducting holes behaving like light-holes with high mobility, small effective mass, and long mean free path. Thus, a larger photoconductive gain and a higher photoconductivity are expected in such a PSL-QWIP.

3.1.4 Experimental

In order to measure the device dark current and spectral responsivity of this PSL-QWIP, a 200×200 μm^2 mesa structure was created by using the chemical etching process. Cr/Au metal films were deposited onto the QWIP mesas with a thickness of about 1500$\mathring{A}$ for ohmic contacts. The substrate of the QWIP device was thinned down to about 50 μm to partially eliminate the substrate absorption screening effect, and polished to mirror-like surface to reduce the reflection of the normal incident IR radiation.

Figure 3.2 shows the dark current versus bias voltage measured at T = 30, 60, and 77 K. The device shows the asymmetrical dark current characteristic under the positive and negative bias, which is attributed to the band bending due to dopant migration effect occurred during the layer growth[17]. This PSL-QWIP is under background limited performance (BLIP) at V_b = 0.3 V, 0.7 V, and T = 75, 60 K respectively, for a field of view (FOV) 90°.

12

The responsivity of this QWIP under normal incidence illumination was measured as a function of temperature, bias voltage, and wavelength using a blackbody radiation source and automatic PC-controlled single-grating monochromater system. Two dominant peaks were detected: a twin peak in the LWIR of $\lambda_{p1,2}$ = 8.9, 8.4 μm was observed, as shown in Fig. 3.3, and the other is in the MWIR of λ_{p3} = 5.5 μm, as shown in Fig. 3.4. The LWIR twin peaks observed at $\lambda_{p1,2}$ = 8.9, 8.4 μm cover a broad wavelength band from 6.5 to 12 μm. Responsivities of 24 mA/W at V_b = 0.3 V and 45 mA/W at V_b = 0.7 V were obtained at T $\leq$ 75 K for the two peak wavelengths. The cutoff wavelength for the LWIR detection band was found to be $\lambda_c \approx$ 10 μm with a spectral bandwidth of $\Delta\lambda/\lambda_p$ = 35%. These twin peak wavelengths are attributed to the intersubband transition between the confined ground heavy-hole state (E_{HH1}) to the continuum heavy-hole states (E_{HH3}), which is resonantly lined up with the type-II light-hole continuum states, as illustrated in Fig. 3.1. The transition energy for these peak wavelengths is in reasonable agreement with the theoretical calculation. These twin peaks broaden the LWIR detection band width by about a factor of 2. The physical origin for the twin-peak feature is not clear, but a possible explanation may be given as follows. When the continuum HH- and LH-bands are strongly mixed, an individual subband (either the HH-band or LH-band) further splits into two subsubbands due to the coupling and interaction: one upward and the other downward. This gives rise to the observed twin-peak feature in the LWIR band. The MWIR peak observed at λ_{p3} = 5.5 μm covering the wavelength ranging from 4 to 6.5 μm. Responsivities for the MWIR band were found to be 7 mA/W, 13 mA/W at V_b = 0.3, 0.7 V and T = 75 K, respectively. The spectral bandwidth of $\Delta\lambda/\lambda$ = 27% was obtained with a cutoff wavelength at λ_c = 6 μm. The intersubband transition occured between E_{HH1} and E_{HH4} subbands was responsible for the MWIR detection. However, no mixing and interaction between HH-band and LH band was observed in this transition. This may be due to the weak overlap interaction at higher subbands. Since E_{HH2} subband is confined inside the quantum wells with very low tunneling probability off the thicker barrier layer, the photoresponse from this heavy-hole state was not detected.

Responsivities versus bias voltage for the LWIR and MWIR peak wavelengths were measured at T = 75 K, and the results are shown in Fig. 3.5 and Fig. 3.6, respectively. In Figure 3.5, the responsivity of λ_{p1} = 8.9 μm (or λ_{p2} = 8.4 μm) increases almost linearly with bias voltage for $V_b \leq$ -1.6V and $V_b \leq$ +1.2V, and then rapidly falls to zero from the maximum value for $V_b \leq$ 0.1V. Similarly, as shown in Fig.3.6, the responsivity for the λ_{p3} = 5.5 μm wavelength falls rapidly to zero for $V_b \leq$ 0.1 V, which is substantially smaller than that of λ_{p1} = 8.9 μm. This rapid falling characteristic of the responsivities provides a direct evidence of the lineup property

13
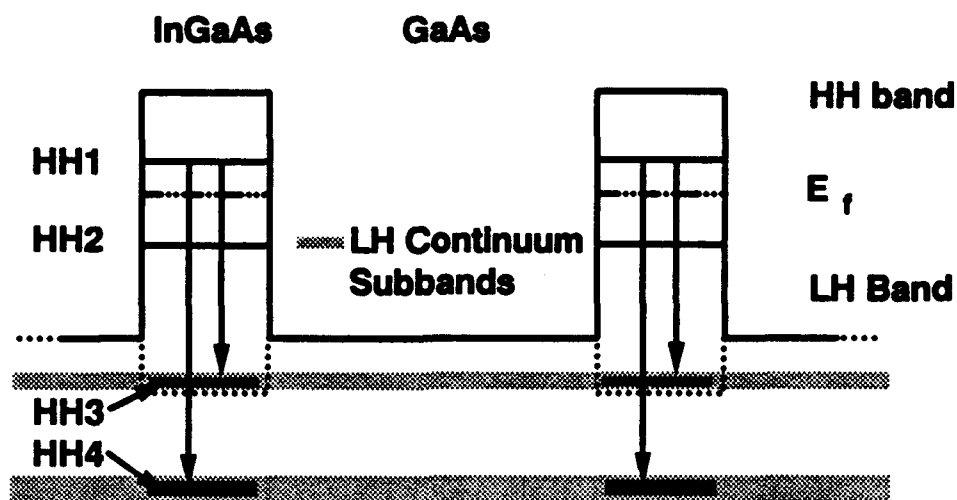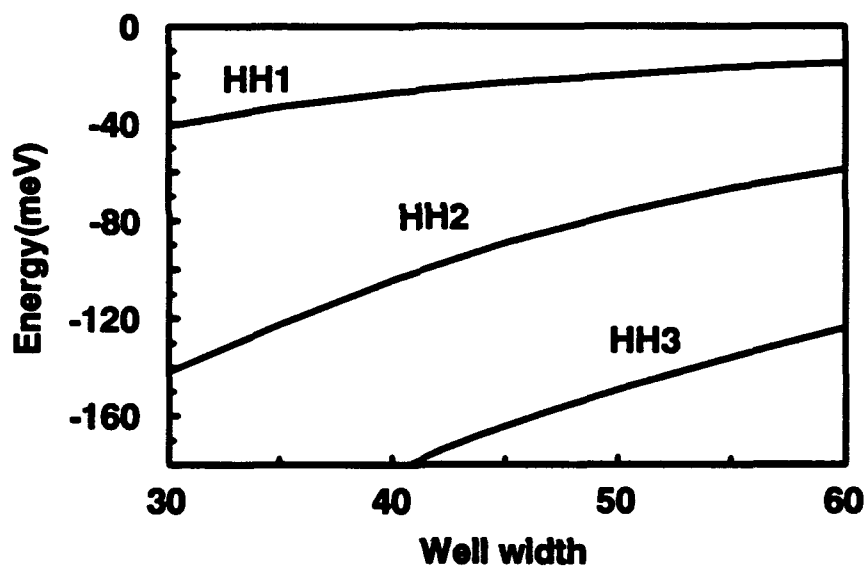
Figure 3.1 (a) Schematic energy band diagram for the In$_{.4}$Ga$_{.6}$As/GaAs
PSL-QWIP, and (b) energy of zone center valence band
subband levels as a function of well width for the p-type
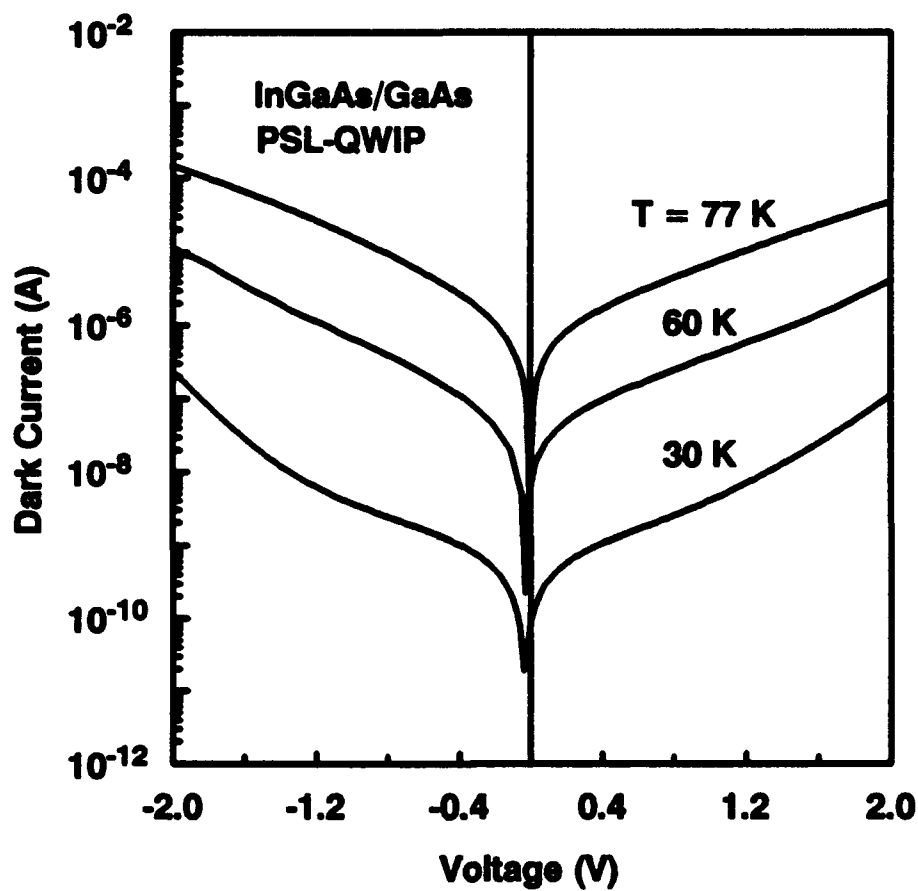compressive strained layer InGaAs/GaAs QWIP.

Figure 3.2 Dark current versus bias voltage measured at T = 30, 60, and 77 K for the In $_{.4}$Ga $_{.6}$As/GaAs PSL-QWIP shown in Fig. 3.1.
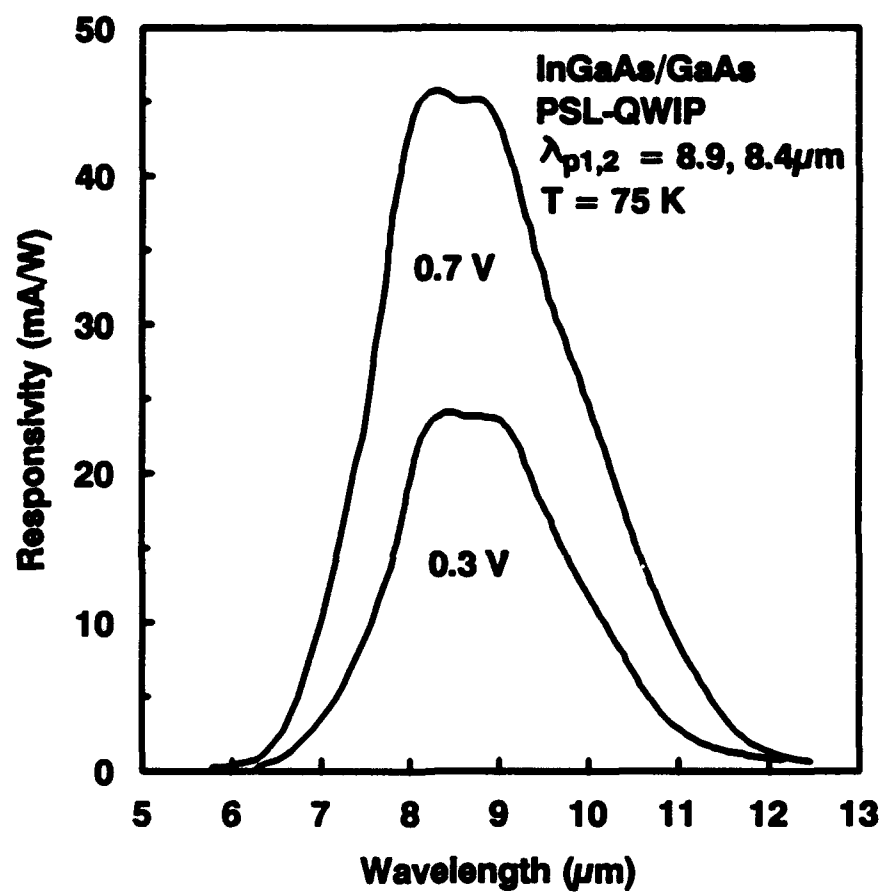
Figure 3.3 Responsivity versus wavelength for the PSL-QWIP shown in Fig. 3.1 for $\lambda_{p1,2}$ peak wavelength measured at Vb = 0.3, 0.7 V and T = 77 K.
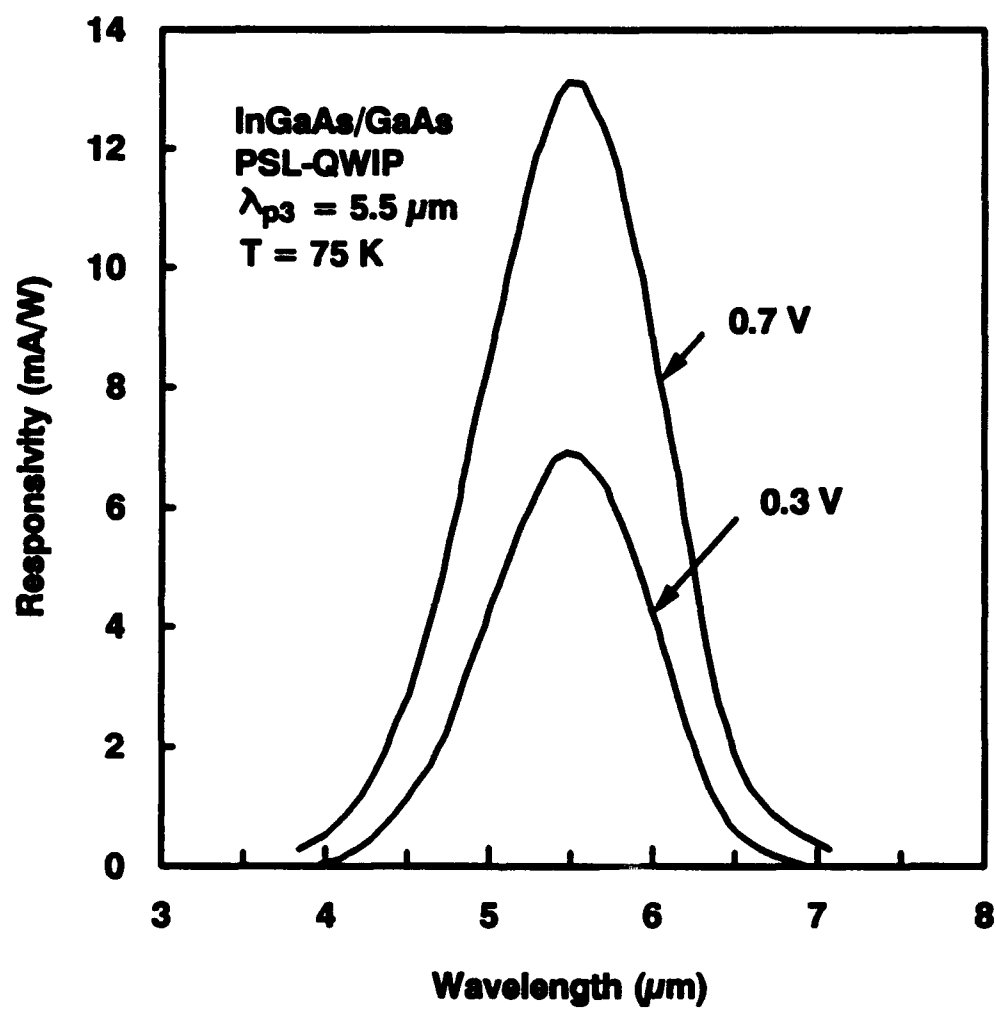
Figure 3.4 Responsivity versus wavelength for the PSL-QWIP shown in Fig. 3.1 for λ_{p3} peak wavelength measured at Vb = 0.3, 0.7 V and T = 77 K.
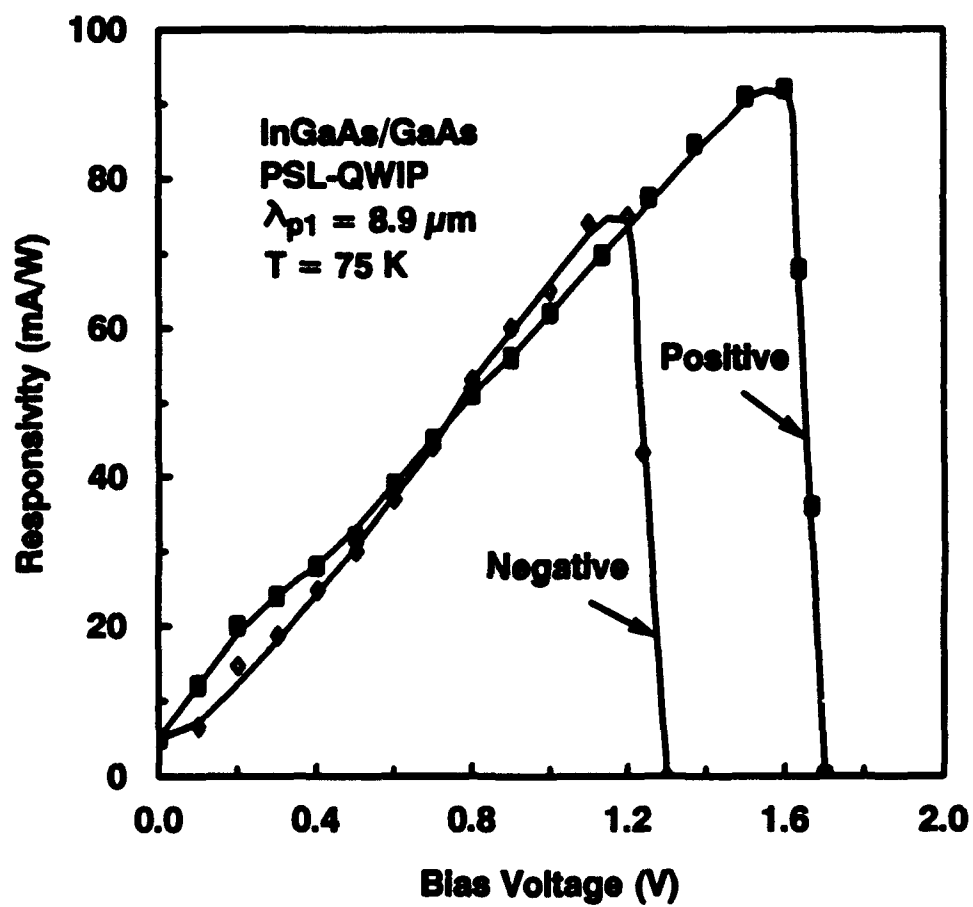
Figure 3.5 Responsivity versus bias for the λ_{p1} peak response measured
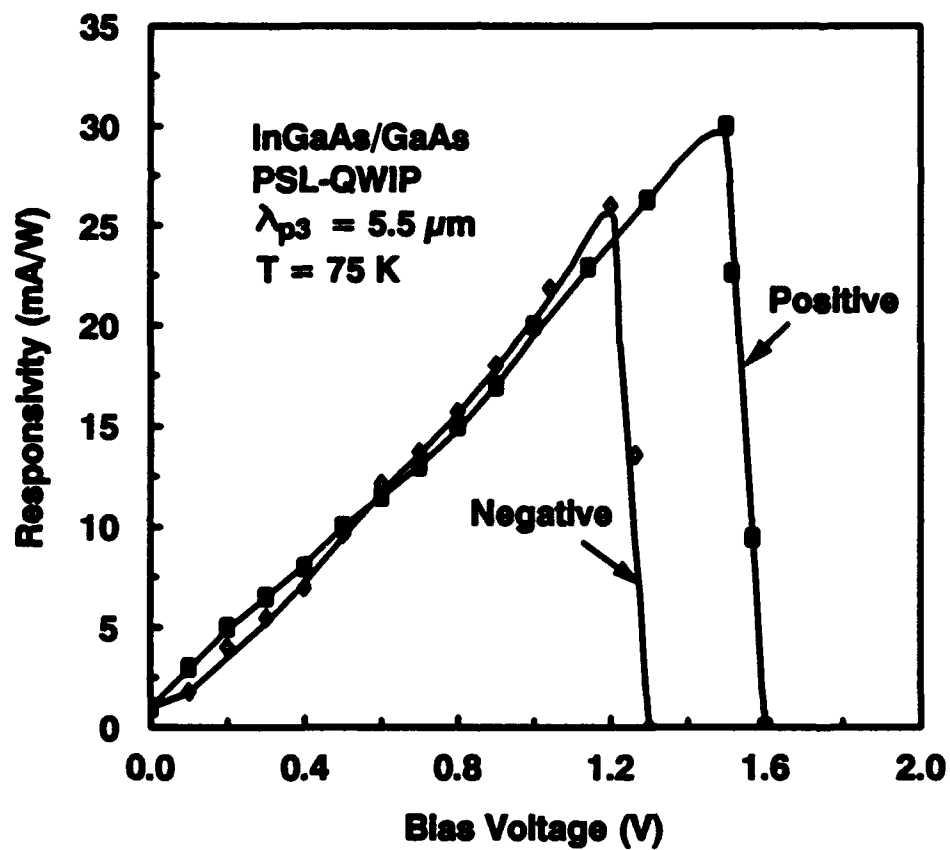at positive and negative bias at T = 75 K.

Figure 3.6 Responsivity versus bias for the λ_{p3} peak response measured at positive and negative bias at T = 75 K.

between the HH-band and the LH-band, which is similar to the performance of n-type BTM QWIPs reported previously by us[18]. It is noted that the responsivity is higher at positive bias than those at negative bias for both the MWIR and LWIR bands when $V_b \leq 0.4$ V. Furthermore, a photovoltaic (PV) response for both MWIR and LWIR bands was also observed for the first time in this PSL-QWIP. However, the PV mode photoresponse observed in this detector may result from a different mechanism other than that from energy band bending effect ascribed in n-type QWIPs[18]. Further study of this effect will be given in next report.

In conclusion, we have demonstrated for the first time a new normal incidence p-type compressive strained-layer InGaAs/GaAs QWIP grown on GaAs substrate for the MWIR and LWIR two-band detection. The intersubband absorption and photoresponse in this PSL-QWIP were enhanced by the biaxial compressive strain in the InGaAs quantum well layers. The improvement in the performance of bandwidth and photo-responsivity in this PSL-QWIP was achieved by using type-I and type-II configuration coupling transport mechanism. Since the total layer thickness of this PSL-QWIP is greater than the coherent strained-layer limitation, certain strain relaxation might occur, which will result in a larger dark current and lower photoresponse than theoretical prediction. By further optimizing the quantum well dopant density, barrier layer thickness, biaxial strain strength, and layer structure parameters, a high performance PSL-QWIP can be developed for the MWIR and LWIR two-color infrared focal plane arrays image sensor systems with background limited performance (BLIP) at T = 85 K temperature operation.

3.2 A GaAs/AlAs/AlGaAs and GaAs/AlGaAs Stacked QWIP for 3-5 and 8-14μm Detection

Summary: A new two-color GaAs/AlAs/AlGaAs and GaAs/AlGaAs quantum well infrared photodetector (QWIP) with photovoltaic (PV) and photoconductive (PC) dual-mode operation at 3-5 and 8-14 μm has been demonstrated. It consists of a stack of the mid-wavelength infrared (MWIR) QWIP and the long-wavelength infrared (LWIR) QWIP. The PV detection scheme uses transition from the ground-state to the first excited state for the MWIR-QWI. The PC detection scheme has two different transitions, one is identical to the PV mode detection scheme and the other uses transition from the ground state to the miniband state of the LWIR QWIP. The peak responsivity at zero bias (PV mode) was found to be 17 mA/W at $\lambda_p = 4.1$ μm and $T = 50$ K with a bandwidth $\Delta\lambda/\lambda_p = 1.5$ %. The peak responsivities for the PC mode were found to be 25 mA/W at $\lambda_p = 4.1$ μm, $V_b = 1.0$ V, and 0.12 A/W at $\lambda_p = 11.6$ μm, $V_b = 3.2$V, and at T = 50 K, with a

bandwidth $\Delta\lambda/\lambda_p = 18$ %. The PV responsivity was found to be 68 % of the PC responsivity at $\lambda_p = 4.1$ μm and $T = 50$ K, demonstrating the ability for efficient PV mode operation at 3-5 μm by using the double barrier quantum well (DBQW) structure. This is the highest ratio reported for the spectral region of 3-5 μm wavelength with a DBQW structure.

3.2.1 Introduction

Recently, with the advances in III-V material growth technologies, quantum well infrared photodetectors (QWIPs)[19-22] have been developed for applications in the infrared focal plane arrays (FPAs) imaging sensor systems.[23,24] Furthermore, multi-color and voltage-tunable QWIPs can be achieved[26-29] using multistack structures, asymmetric and symmetric quantum well structures. Nearly all of the QWIPs are operating on the photoconductive (PC) mode detection. However, significant photovoltaic (PV) effects in the QWIPs have been reported in the literature.[29-33] The PV mode operation is promising for practical applications, since the suppression of the dark current strongly improves the noise properties. However, the responsivity of the PV mode is significantly smaller than that of the PC mode. Therefore, improvement in the performance of PV QWIPs is highly desirable for using such detectors in the infrared FPA image sensor applications.

In this section we report a new two-color stack GaAs/AlAs/AlGaAs and GaAs/AlGaAs QWIP with PV and PC dual-mode operation at 3-5 and 8-14 μm. The QWIP layer structure was grown on a semi-insulating (SI) GaAs substrate by using the molecular beam epitaxy (MBE) technique. The quantum wells consist of two stacks designed as a mid-wavelength QWIP (MW-QWIP) and a long-wavelength QWIP (LW-QWIP). Figure 3.7 shows the entire layer structure of this two-stack QWIP. A 0.7-μm GaAs buffer layer (doped to $n = 2.0 \times 10^{18}$ cm^{-3}) was first grown on the SI GaAs substrate as an ohmic contact layer, followed by the growth of the first stack, designed as a MW-QWIP with a 20-period of GaAs/AlAs/AlGaAs double barrier quantum wells[34,35] (DBQW) with a well width of 50 Å(doped to $n = 1.5 \times 10^{18}$ cm^{-3}) and two undoped barriers which were of 14 Å AlAs inner barrier and 300 Å Al$_{0.3}$Ga$_{0.7}$As outer barrier. A second GaAs buffer layer of 0.5-μm thick (doped to $n = 2.0 \times 10^{18}$ cm^{-3}) was then grown on top of the first QWIP as an ohmic contact layer, followed by the growth of the second stack, designed as a LW-QWIP, with a 21-period of GaAs/AlGaAs quantum wells with a well width of 88 Å and a dopant density of 1.5×10^{18} cm^{-3}. The barrier layer on each side of the GaAs quantum wells consists of a 8-period undoped Al$_{0.3}$Ga$_{0.7}$As (50 Å)/GaAs (28 Å) superlattice layer which were grown alternatively with the GaAs quantum wells. Finally, an n$^+$- GaAs cap layer of 0.3 μm thick with a dopant density of 2×10^{18} cm^{-3} was

21

grown on top of the QWIP layer structure to facilitate the top ohmic contact. The DBQW structure of the MW-QWIP offers a PV mode detection with excellent detection characteristics which are comparable to the PC mode QWIPs. The physical parameters of the LW-QWIP are chosen so that the first excited level E_2 is lined up within the miniband E_{SL} on both sides of the quantum well to obtain a maximum intersubband absorption strength. In order to minimize the undesirable tunneling current through the barrier layers, a 8-period undoped $Al_{0.3}Ga_{0.7}As$ (50 Å)/GaAs (28 Å) superlattice layer was used in this LW-QWIP structure to suppress the tunneling current from the heavily populated ground state E_1 in the quantum wells.

3.2.2. Results and Discussion

The 2-color QWIP mesa structure with an active area of 200×200 μm^2 was created by chemical etching through the two-stack quantum well active layers and stopped at the 0.7-μm thick heavily doped GaAs buffer layer for ohmic contact. A square contact ring composed of AuGe/Ni/Au materials was first deposited around the periphery of the mesa and alloyed for ohmic contact formation. To enhance the light coupling efficiency in the quantum well, we used a 2-D double periodic square mesh metal grating coupler[36] on the QWIP for normal incident illumination. As discussed in the previous quarterly report, we found that $g = 4$ μm(where g is the grating period) and $a/g = 0.5$ (where a is the width of square aperture in the metal mesh) are the optimum grating dimension and period for this 2-color QWIP. The metal grating was then deposited within the interior of the contact ring by using electron beam evaporation of Au followed by lift-off process.

Figure 3.8 shows the energy band diagram of this 2-color QWIP structure, which also illustrates the bound-to-miniband (BTM) and bound-to-quasi-bound (BQB) transition schemes for the two-color detection. The first transition scheme is from the localized ground-state E_1 to the first quasi-bound state E_2 in the GaAs quantum well of the MW-QWIP stack. The second transition scheme is from the localized ground-state E_1 to the miniband E_{SL} in the GaAs quantum well of the LW-QWIP stack. To analyze these transition schemes, we performed theoretical calculations of the energy levels of the bound states and continuum states and the transmission probability $|T * T|$ for this detector using a multi-layer transfer matrix method[3], and the results are shown in Fig.3.9. For comparison, we have also included in Fig. 3.9 the transmission probability for a single quantum well with the same barrier width of the bulk barrier. Considering the effects due to depolarization and the electron-electron interaction, we obtain two response peaks, one at $\lambda = 3.9$ μm and the other at $\lambda = 11.7$ μm.

To understand the behavior of this 2-color QWIP, we first prepared two samples with BTB and BTM quantum structures mentioned above separately. The MW-QWIP (BTB) and LW-QWIP (BTM) represent the the first stack and the second stack of this 2-color QWIP structure, respectively. Fig.3.10 shows the dark current versus bias voltage (I-V) curves of the MW-QWIP and the LW-QWIP measured at T = 30, 50, and 77 K. The results show that the dark current of the LW-QWIP is higher than that of the MW-QWIP at the same bias. This is due to the fact that the LW-QWIP has a shallower quantum well and the thermal-generated electrons can escape more easily from the quantum wells. Therefore, based on the I-V curves shown in Fig.3.10, we can see that when the two stacks are combined to form a 2-color detector, most of the voltage drop is across the MW-QWIP stack at low bias ($<$ 1.5 V). Therefore, a high field domain always forms first in the MW-QWIP stack. The voltage drop across the LW-QWIP stack becomes significant only when the bias is greater than 1.5 V.

Figure 3.11 shows the dark current-voltage (I-V) for the 2-color stacked QWIP measured at T = 30, 50, and 77 K. It is noted that the 300 K background photocurrent curve (dashed) crosses the dark I-V curve at $V_b = -0.65$ V and $T = 50$ K. Thus, the background limited performance (BLIP) condition occurs at $T \leq 50K$ and $V_b \leq 0.6$V. The 300 K background photocurrent can be obtained from

$$I_B = A \int_{\lambda_1}^{\lambda_2} R(\lambda)S(\lambda)d\lambda \qquad (6)$$

where A is the device area, $R(\lambda)$ is the responsivity curve, λ_1 and λ_2 are the limits of the integration, and the blackbody power spectral density is given by

$$S(\lambda) = (2\pi hc/\lambda^5)(e^{hc/\lambda kT} - 1)^{-1} \qquad (7)$$

Using $A = 4 \times 10^{-4}$ cm^2, $R_p = 0.018$ A/W (at $\lambda = 4.1$ μm, $V_b = 0$ V, and $T = 30$ K), and $T = 300$ K gives a total calculated 300 K background photocurrent of $I_B = 0.12$ nA. This is in good agreement with the measured photocurrent of $I_B = 0.3$ nA (as shown in Fig.3.11). Therefore, at $T = 50$ K this 2-color detector is under BLIP condition only in the PV mode operation, but not the PC mode operation.

Figure 3.12 shows the bias dependent responsivity and detectivity for the single LW-QWIP measured at $\lambda_p = 11.6$ μm and $T = 50$ K. The peak responsivity $R_A = 0.14$ A/W was obtained at $V_b = 1.5$ V. From the measured responsivity and dark current, we calculate the detectivity D* using the formula: $D_\lambda^* = R_A(A\Delta f)^{1/2}/i_n$, where A is the effective area of the detector, Δf is the noise bandwidth. The dark current shot noise i_n is given by $i_n = \sqrt{4qI_dg\Delta f}$, where g is the optical

gain, and may be evaluated from the measured responsivity $R_A = \eta \lambda g / 1.24$ and the unpolarized quantum efficiency which was found to be equal to 18 %. Optical gain can also be derived from the noise measurement. The results yielded a peak detectivity $D^*_\lambda = 1.23 \times 10^9$ cm $\sqrt{Hz}$/W at $\lambda_p = 11.6$ μm, $V_b = 3.0$ V, and $T = 50$ K for the PC mode operation.

The spectral response of the 2-color QWIP was measured under back illumination as a function of temperature and bias voltage (V_b) using a 0.25 m grating monochromator with a 1273 K blackbody source. The normalized spectral responsivity measured at $V_b = 0, 3.2$ V and $T = 50$ K is shown in Fig.3.13. Two response peaks were observed: one at $\lambda = 4.1$ μm with $V_b = 0$ V and the other at $\lambda = 11.6$ μm with $V_b = 3.2$ V. The peak wavelengths are in good agreement with our theoretical calculations. The bias dependence of the responsivity at $T = 50$ K is shown in Fig.3.14. It is noted that the photoresponse of the MW-QWIP stack is dominated at low bias and saturated above $V_b = 1$ V, When $V_b > 1.5$ V, the LW-QWIP stack starts to work and reaches a maximum value at $V_b = 3.2$ V. The results show the potential of this 2-stack QWIP structure as a 2-color QWIP with a PV and PC dual-mode operation at 3-5 μm and 8-14 μm. The peak responsivity at zero bias (PV mode) was found to be 17 mA/W at $\lambda = 4.1$ μm and $T = 50$ K, with a bandwidth $\Delta\lambda/\lambda_p = 1.5$ %. Two peak responsivities were found on the PC mode, one was 25 mA/W at $\lambda_p = 4.1$ μm, $V_b = 1.0$ V, and $T = 50$ K, the other was 0.12 A/W at $\lambda_p = 11.6$ μm, $V_b = 3.2$ V, $T = 50$ K, and the bandwidth $\Delta\lambda/\lambda_p = 18$ %. The PV responsivity was found to be 68 % of the PC responsivity at $\lambda_p = 4.1$ μm and $T = 50$ K. This is one of the highest ratios reported in the spectral region of 3-5 μm for the QWIPs. The PV response has been interpreted due to the doping migration effect[33] with further enhancement by the DBQW structure. Since the dark current of the PV mode operation QWIP is much smaller than that of the PC mode, one can achieve a better performance in QWIP by using PV mode detection at 3-5 μm.

In conclusion, we have demonstrated a new two-color stacked GaAs/AlAs/AlGaAs BTB and GaAs/AlGaAs BTM QWIP with PV and PC dual-mode operation at 3-5 and 8-14 μm. The PV detection scheme uses transition from the ground-state to the first excited state of the MW-QWIP. The PC detection scheme has two different transitions, one is similar to the PV detection scheme and the other uses transition from the ground state to the miniband of the LW-QWIP. The peak responsivity at zero bias (PV mode) was found to be 17 mA/W at $\lambda_p = 4.1$ μm, $T = 50$ K, with a bandwidth $\Delta\lambda/\lambda_p = 1.5$ %. Two peak responsivities for the PC mode detection, were found to be 25 mA/W at $\lambda_p = 4.1$ μm, $V_b = 1$ V, and $T = 50$ K, and 0.12 A/W at $\lambda_p = 11.6$ μm, $V_b = 3.2$ V, $T = 50$ K, and the bandwidth $\Delta\lambda/\lambda_p = 18$ %. The PV responsivity was found to be 68 % of the

```
┌─────────────────────────────────────────────┐
│  0.3 μm GaAs n=2E18 cm-3                      │
├─────────────────────────────────────────────┤
│              ⋮                                │
├─────────────────────────────────────────────┤  ⎫
│  88 Å GaAs n=1.5E18 cm-3                      │  │
├─────────────────────────────────────────────┤  │
│  50 Å Al₀.₃Ga₀.₇As undoped                    │  │
├─────────────────────────────────────────────┤  │
│              ⋮                                │  ⎬ X 21
├─────────────────────────────────────────────┤  │
│  28 Å GaAs undoped                      ⎫     │  │
├─────────────────────────────────────────┬ X 7 │  │
│  50 Å Al₀.₃Ga₀.₇As undoped              ⎭     │  │
├─────────────────────────────────────────────┤  ⎭
│  0.5 μm GaAs n=2E18 cm-3                      │
├─────────────────────────────────────────────┤
│              ⋮                                │
├─────────────────────────────────────────────┤  ⎫
│  300 Å Al₀.₃Ga₀.₇As undoped                   │  │
├─────────────────────────────────────────────┤  │
│  14 Å AlAs undoped                            │  ⎬ X 20
├─────────────────────────────────────────────┤  │
│  50 Å GaAs n=1.5E18 cm-3                      │  │
├─────────────────────────────────────────────┤  │
│  14 Å AlAs undoped                            │  ⎭
├─────────────────────────────────────────────┤
│  buffer 0.7 μm GaAs n=2E18 cm-3               │
├─────────────────────────────────────────────┤
│                                               │
│  SI GaAs Substrate                            │
│                                               │
└─────────────────────────────────────────────┘
```
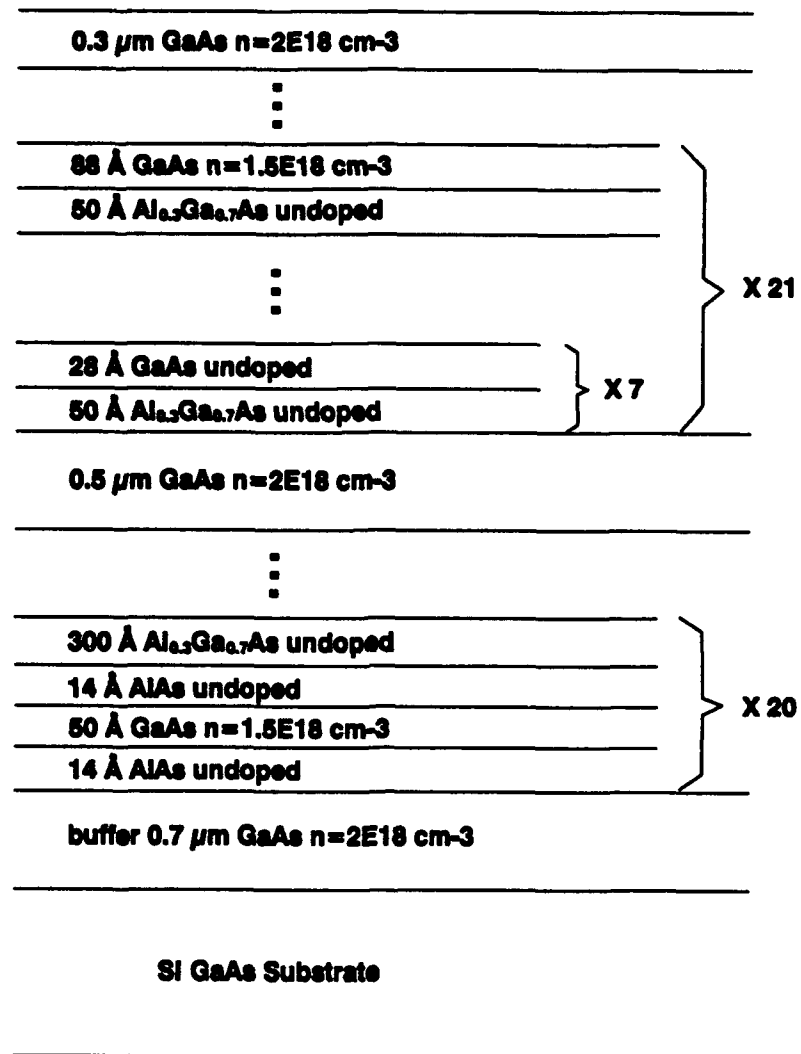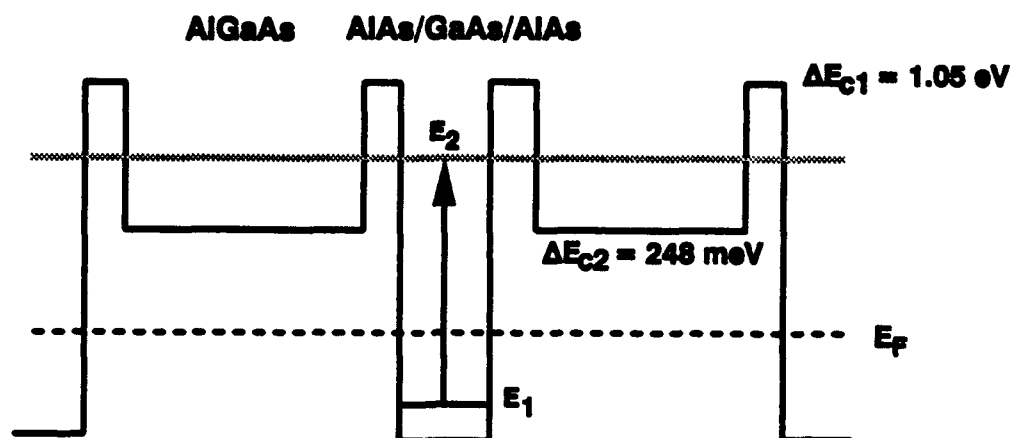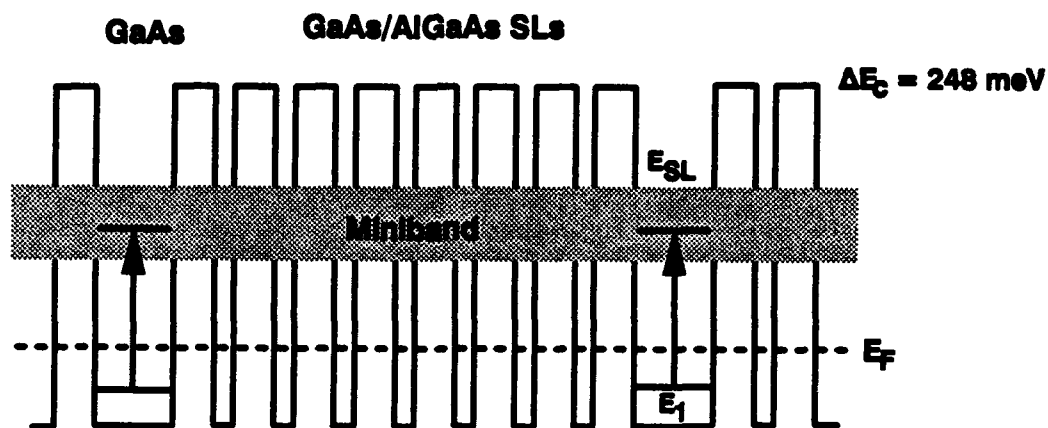
Figure 3.7 The quantum well layer structure for the 2-color MW BTB QWIP and LW BTM QWIP.

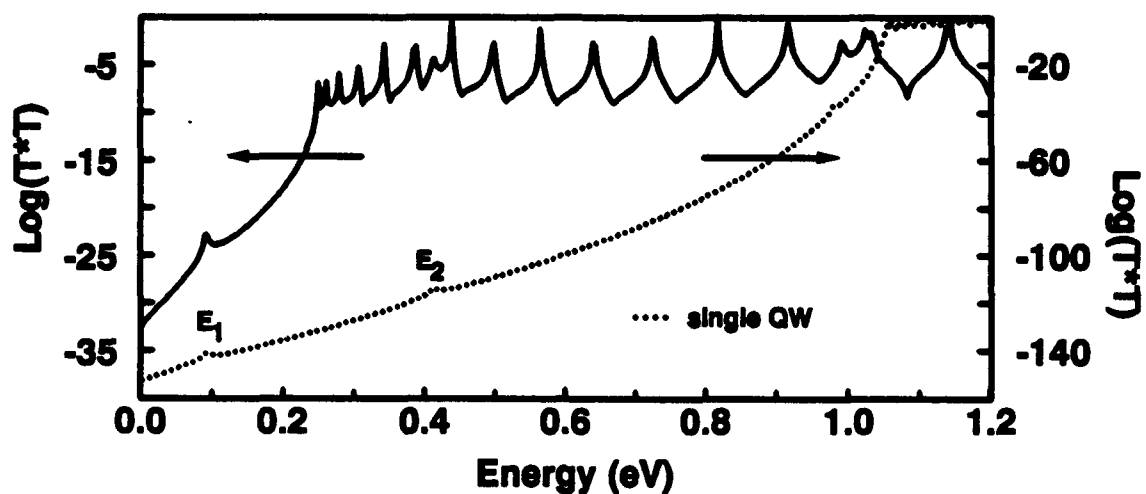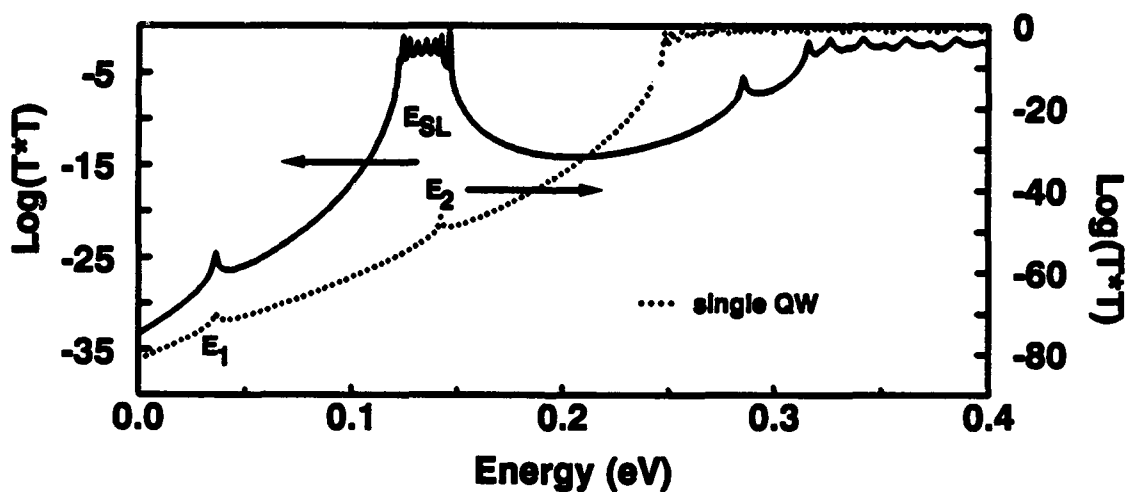**Figure 3.8** The schematic energy band diagram for the 2-color QWIP structure, (a) MW-QWIP stack and (b) LW-QWIP stack.

26

(a) MW-QWIP stack

(b) LW-QWIP stack

Figure 3.9 The calculated energy states and transmission coefficient –
$T * T$– for the 2-color QWIP structure by using the multiple-
layer transfer matrix method: (a) MW-QWIP stack and (b)
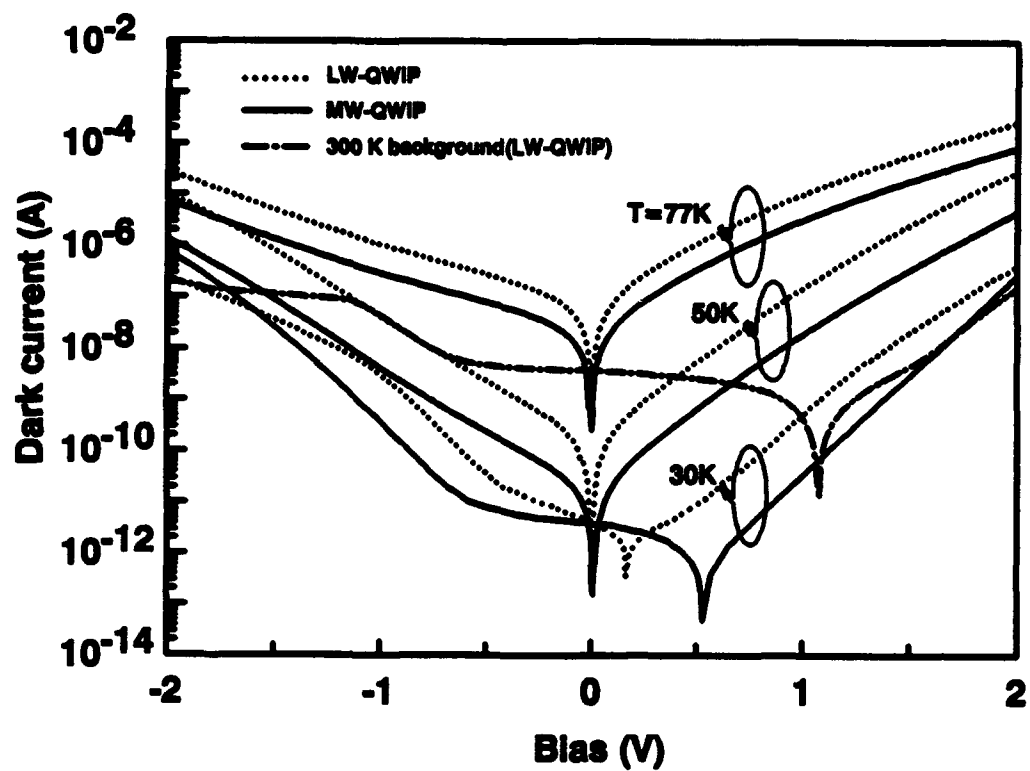LW-QWIP stack.

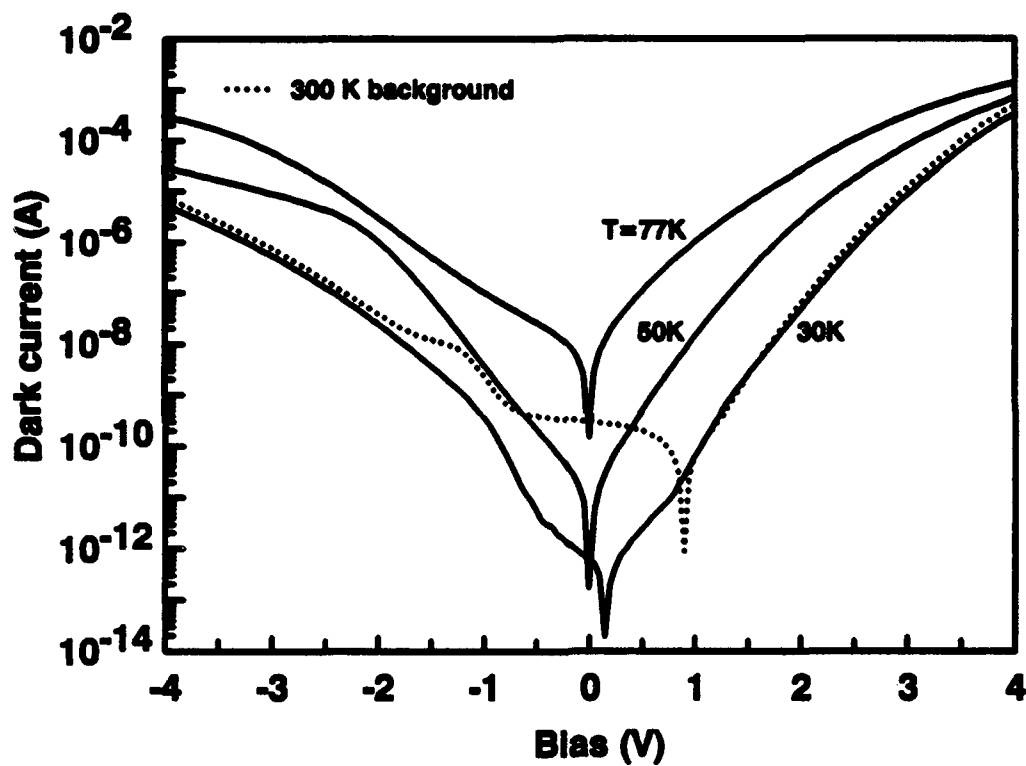**Figure 3.10** The dark current versus bias voltage and temperature for the single LW-QWIP and single MW-QWIP.

28

Figure 3.11 The dark current versus bias voltage and temperature for the 2-color stack QWIP.

29
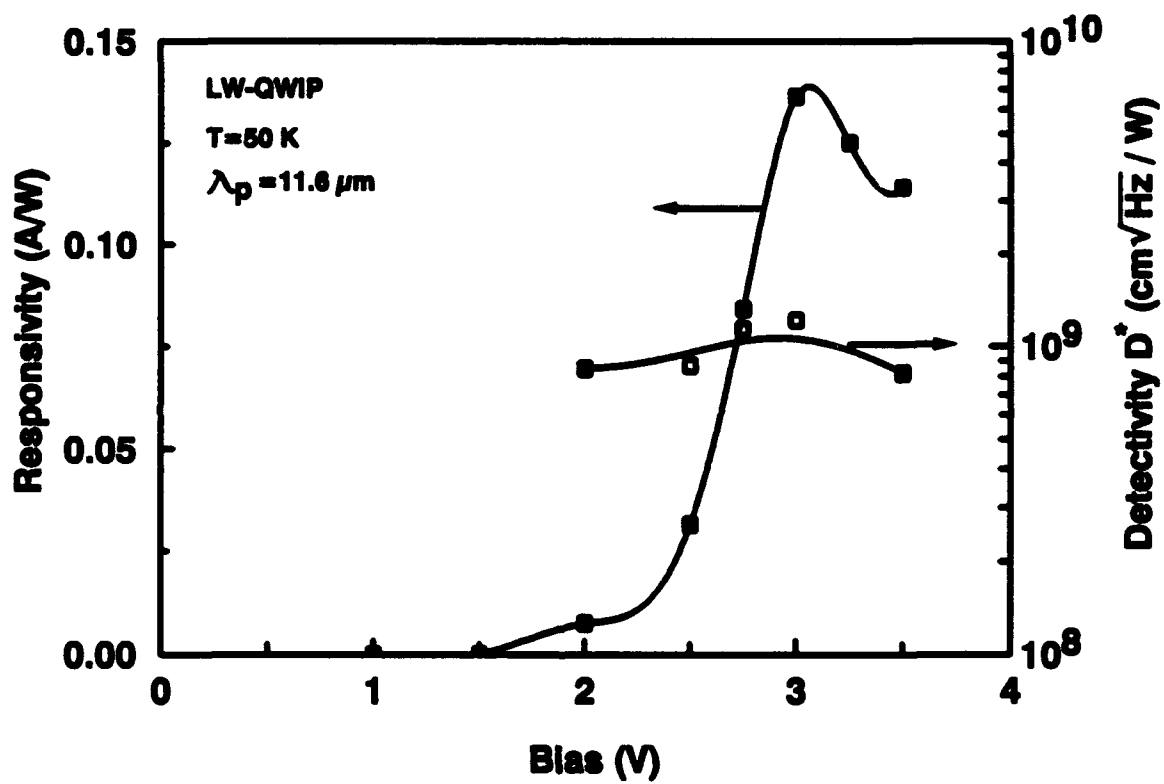
Figure 3.12 Bias dependence of the peak responsivity and detectivity for
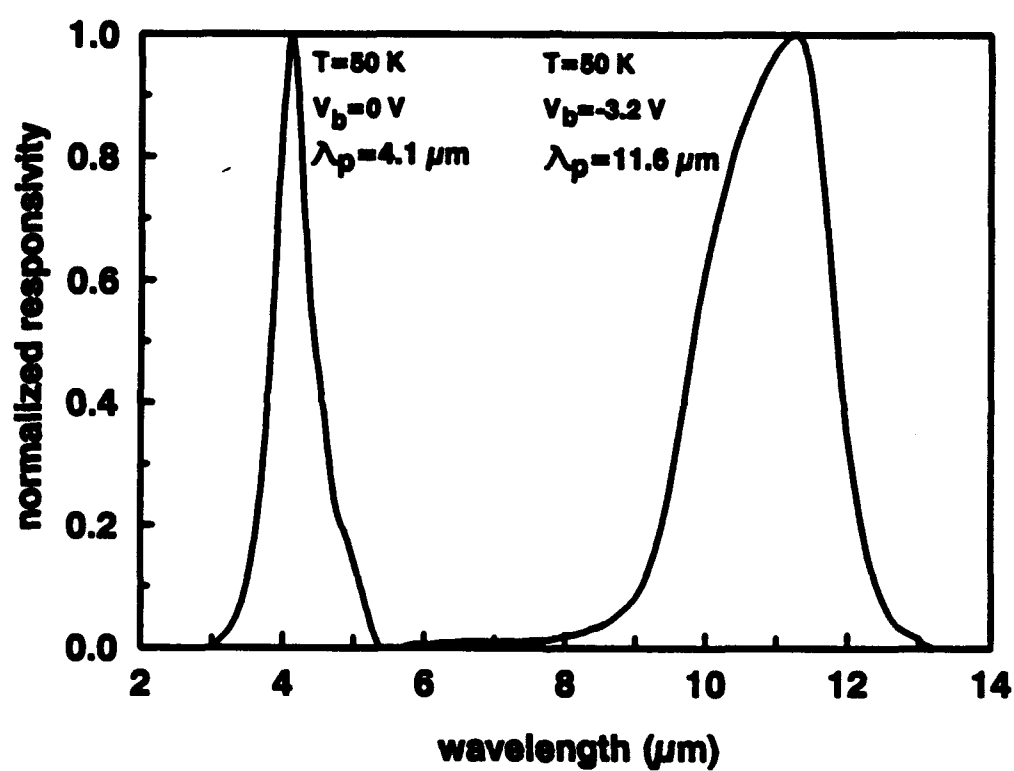the single LW-QWIP at $T = 50$ K.

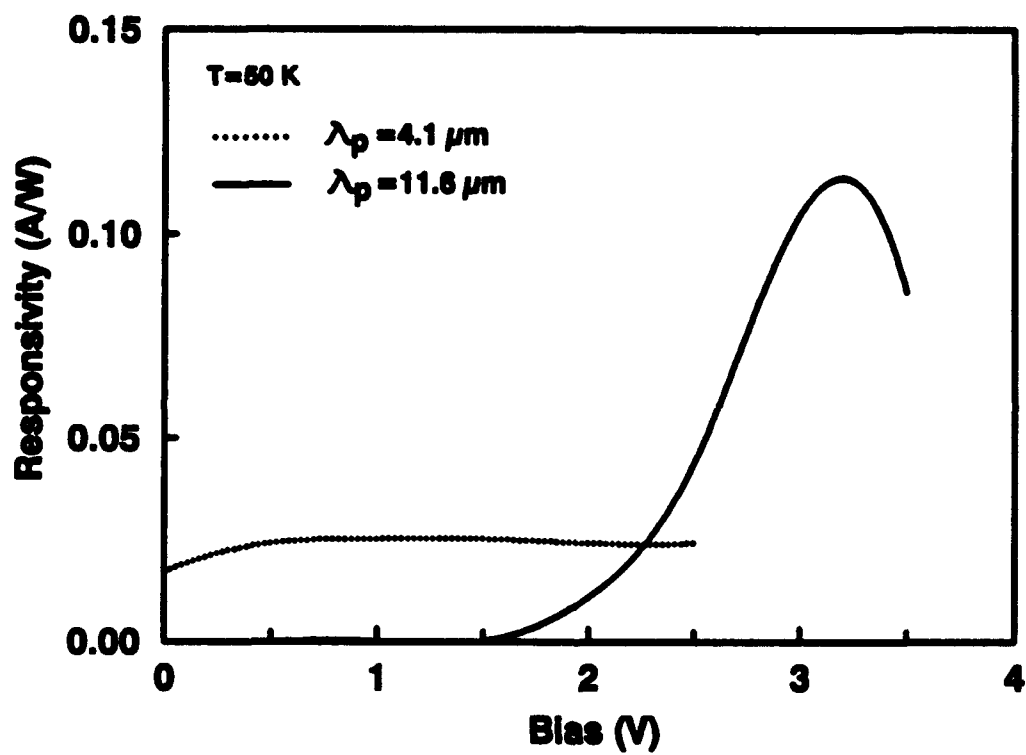**Figure 3.13** Normalized responsivity versus wavelength for the 2-color stack QWIP measured at $T = 50$ K.

Figure 3.14 The peak responsivity versus bias voltage for the 2-color stack
QWIP measured at $T = 50$ K.

PC responsivity at $\lambda_p = 4.1$ μm and $T = 50$ K, demonstrating the ability for an efficient PV mode operation at 3-5 μm. The results reported here represent only a preliminary design of the 2-color detector. Further improvement on the performance of the 2-color stack QWIP is expected to raise the operating temperature to $T = 77$ K for practical focal plane arrays image sensor applications.

3.3 Design of An Optimum Performance BTM QWIP

Summary: Analysis of the quantum well detector parameters for achieving the optimum performance in a bound-to-miniband (BTM) transition QWIP has been made in this study. The reduction of dark current was achieved by either increasing the superlattice barrier height or by adding a blocking barrier layer to the QWIP. To increase intersubband absorption in the quantum wells, a 4 μm thick of AlAs cladding layer beneath the detector active region is employed to form a waveguide geometry for the QWIP. This waveguide coupling scheme further enhances the QWIP absorption due to multi-pass of IR radiation along the wave propagating direction. Based on our experimental study, the optimum quantum well period was found to be 18 for an InGaAs BTM QWIP with waveguide and 20 for the same QWIP without waveguide.

3.3.1 Introduction

In this section, we describe a theoretical and experimental study of the procedures for optimizing the performance of a BTM QWIP. The effects of device structure and the parameters such as the barrier height and well width, quantum well doping concentration and quantum well period, and the waveguide layer thickness on the performance of a BTM QWIP are analyzed.

3.3.2 General Consideration of a BTM QWIP

The ability to control the IR spectral response bandwidth by varying the material compositions and quantum well parameters is a key feature for the QWIP devices. The bound-to-continuum (BTC) and bound-to-miniband (BTM) transition QWIPs are the two QWIP structures which have been developed for the LWIR focal plane arrays (FPAs) applications. By varying the well width and compositionally controlled the barrier height, the response wavelengths of the intersubband transitions in these QWIPs can be readily changed over a wide range of MWIR and LWIR spectrum. Although the BTC and BTM QWIP structures are quite different, the operation of a BTC QWIP is very similar to that of a BTM QWIP. The infrared radiation is absorbed in the doped quantum wells, exciting an electron from the highly populated ground state and transporting via the miniband states or the continuum states until it is collected at the electrodes or recaptured into another

quantum well. The main difference in the operation of these two types of QWIPs is that the transport occurs in the high-mobility continuum states above the barrier for the BTC QWIPs, while transport is via the global miniband states inside the quantum well for the BTM QWIPs.

The use of superlattice barrier layer in a BTM QWIP is to increase the barrier height and to form a miniband inside the quantum well. This could lead to a significant reduction of the thermionic emission dark current over the barrier, and hence should raise the operation temperature of a QWIP. Higher operation temperature is desirable for practical applications of BTM QWIPs LWIR detection and focal plane arrays. In a BTM QWIP, the superlattice barrier can be made very thin to allow the formation of low-lying minibands corresponding to long wavelength, and, to facilitate the transport of carriers through the superlattice. Under small bias voltage, the photocurrent is mainly due to the tunneling between wells which can be controlled by varying the barrier thickness of the superlattice well, i.e., thin and high barriers allow broadband detection with lower dark current. It is also worth noting that for photoconductive detectors, the absorption spectrum was found to be much broader for the BTC QWIP than that of the BTM QWIP. As a result, the absorption constant of the former is significant smaller than that of the latter.

3.3.2 Barrier Height and $Al_xGa_{1-x}As$ Composition

To reduce the dark current of a QWIP, a higher barrier height is needed in the quantum well. In a GaAs/$Al_xGa_{1-x}As$ BTM QWIP, this can be achieved by choosing the aluminum composition x to be 0.38, which would yield a barrier height of 283 meV for the quantum well. The well width is determined so that there are only two subband levels in the quantum well with energy separation equal to the photon energy corresponding to an intersubband transition peak wavelength of around $10\mu m$ after taking the correction of exchange energy into consideration.[38] The structure described here is illustrated in Fig.3.15. The enlarged GaAs quantum well has a well width of $93\AA$ with two bound states located at E_{W1}, E_{W2} = 35, 140 meV above the conduction band edge of the GaAs quantum well, respectively.

3.3.3 Superlattice Barrier Width

By using a short period superlattice of $Al_{0.38}Ga_{0.62}As$/GaAs as the barrier layer for the BTM QWIP, the width of the superlattice well is determined so that only one miniband state exists in the superlattice well, which overlaps with the first bound excited state of the quantum wells and creates a global miniband for carrier transport. A well width of $28\AA$ for the GaAs superlattice well

34

would meet this requirement. The spectral response bandwidth depends on the barrier width of the superlattice wells.[39] For example, for a 2μm FWHM absorption bandwidth, the barrier width of the superlattice well was found to be equal 49$\AA$, and a miniband width of 20 meV was obtained for such a BTM QWIP.

A dramatic improvement in the BTM QWIP performance can be achieved by increasing the total barrier width from $L_b = 300\AA$ to 500$\AA$.[40] This is due to a strong reduction in thermally assisted tunneling with increasing barrier width, which leads to a large reduction in dark current. Further increase of barrier width gives virtually the same detectivity D^*.[41] This is due to the fact that reduction in tunneling due to thicker barrier is partially compensated by the necessity of using a higher bias voltage (which increases the dark current) in order to increase the gain. For this reason, seven periods of Al$_{0.38}$Ga$_{0.62}$As(49 $\AA$)/GaAs(28 $\AA$) superlattice barrier layer is chosen as the optimum value, which yields a total superlattice barrier layer width of 511 $\AA$.

3.3.4 Doping Density in the Quantum Well

The detectivity of a QWIP is nearly constant over a broad doping concentration ($N_D = 10^{16}$ to 10^{18} cm^{-3}) range in the quantum well.[42] Thus, fabrication of large area QWIP arrays can take advantage of this doping independent feature, since it implies that D^* will remain highly uniform across a large 2-D array even the doping density varies across the wafer (for the MBE growth, it is about 1%). On the other hand, filling of the charge storage wells in the multiplexer circuit by the dark current must be avoided, specially for large 2-D arrays. Therefore, it is advantageous to lower the doping density in the quantum well to reduce the dark current while maintaining the same detectivity. However, the absorption intensity is directly proportional to N_D,[39] lowering the doping will also reduce the intersubband absorption intensity. Therefore, a compromised doping density of $N_D = 7 \times 10^{17}$ cm^{-3} is chosen for optimum performance.

3.3.5 Quantum Well Period

We next consider the quantum well period versus the performance of a BTM QWIP. Based on the photocurrent gain mechanism[43,44], the photocurrent gain g in a QWIP can be written as

$$g = \frac{L}{l} = \frac{L}{Nl_w + (N+1)l_b} \propto \frac{1}{N}, \tag{8}$$

where L is the hot-carrier recapture mean free path, l is the total width of the quantum well region, l_w is the width of the quantum well, l_b is the barrier width of the superlattice barrier, and N is the period of multiquantum wells. It is worth noting that a study by Steele et al.[45] on a set of

standard GaAs QWIPs with 4, 8, 16, and 32 periods of quantum wells also found g is inversely proportional to N as predicted by Eq.(8). Increasing N in the quantum well structure will produce two opposing effects: (i) the quantum efficiency η can be enhanced by increasing N (larger l), since the absorption path increases, and (ii) reducing l can increase the gain substantially, since there is a decrease in retrapping of photo-electrons into downstream wells. Therefore, it is useful to study the effect of quantum well period on the responsivity, dark current, and detectivity of a BTM QWIP.

In this section we study the performance characteristics versus quantum well period for three $In_{0.07}Ga_{0.93}As$ BTM QWIPs with quantum well periods of 20, 15, and 4. The devices are labeled as 20-PD, 15-PD, and 4-PD QWIP, respectively.

The InGaAs BTM QWIP structure consists of an n-doped $In_{0.07}Ga_{0.93}As$ quantum well with a well width of 101Å and a doping density $N_D = 1.4 \times 10^{18}$ cm^{-3} and a 5-period undoped $Al_{0.4}Ga_{0.6}As(30\ \text{Å})/GaAs\ (59\ \text{Å})$ superlattice barrier with a total quantum well period of 20, as shown in Fig.3.15. The 15-PD and 4-PD QWIPs were obtained by etching the 20-PD QWIP down to the sixteenth and fifth well region followed by the AuGe/Ni/Au films deposition to form ohmic contacts. The dark current versus bias voltage characteristics measured at 77 K for these samples are shown in Fig. 3.16. Since the dark current in these detectors depends on the applied electric field [46] (i.e., the voltage drop per period), the bias voltage V_b needs to be converted to unit of electric field to take into account the number of barriers in each detector. For this reason, the bias voltage for the 20-PD, 15-PD and 4-PD QWIPs has a ratio of 21 : 16 : 5.

In the present study, the spectral response for the three BTM QWIPs was measured by using a globar, a 7-15μm optical filter, a grating monochromator, and a lock-in amplifier system. The spectral responsivity versus wavelength for these three QWIPs was measured at 77 K and the same bias field (0.1 V/period), and the results are shown in Fig. 3.17. It is interesting to note that the peak spectral responsivity for the 4-PD, 15-PD, and 20-PD QWIPs is almost identical which occurs at $\lambda_P = 10.5\ \mu$m. The responsivities determined by comparison with a calibrated pyroelectric detector were found to be $R_I(\text{4-PD}) = 0.38$ A/W (at $V_b = 0.5$ V), $R_I(\text{15-PD}) = 0.41$ A/W (at $V_b = 1.6$ V), and $R_I(\text{20-PD}) = 0.33$ A/W (at $V_b = 2.1$ V). The noise current i_n in these detectors was measured at $V_b = 0.1$ V/period. It is shown that i_n is limited by the shot noise of the dark current given by[43]

$$i_n = \overline{4qI_Dg\Delta f} \tag{9}$$

where Δf is the noise bandwidth. Combining the noise measurement and the dark current shown

in Fig.3.16 we can deterrmine the gain experimentally, which yields g(4-PD) = 1.2, g(15-PD) = 0.2 and g(20-PD) = 0.1 at V_b = 0.1V/period, respectively. To relate the responsivity R_I to quantum well period N, R_I is written as

$$R_I = \eta g \frac{\lambda}{1.24} = k_1 \frac{1 - e^{\alpha l_w N}}{N l_w + (N+1) l_b} \tag{10}$$

where k_1 is a constant, α is the absorption constant, the numerator is proportional to quantum efficiency η, and the denominator is equal to the length of the multiquantum well region. The calculated responsivity and detectivity versus quantum well period N curves for the three BTM QWIPs are shown in Fig. 3.18. In this figure, the experimental data are labeled by the square dots and stars; solid and dashed lines are the calculated curves. Similar to Eq.(10), the detectivity D^* can be expressed as

$$D^* = \frac{R_I}{i_n} \overline{\sqrt{A_d \Delta f}} = k_2 \frac{1 - e^{\alpha l_w N}}{N l_w + (N+1) l_b} \tag{11}$$

where k_2 is a constant and A_d is the detector area. The calculated and measured detectivities versus quantum well period N are also shown in Fig. 3.18. The difference between the measured data and theoretical prediction can be attributed to the uncertainty in etching process of the 4-PD and 15-PD QWIP devices. The exact etching depth is very difficult to determine by using the simple DEKTAK IIA depth profile measurements, which has an error range about $\pm 300 \overset{\circ}{A}$ corresponding to one quantum well period. Nevertheless, the theoretical predictions are in good agreement with those obtained directly from the measurements. Although the responsivity of the 4-PD QWIP is larger than that of the 20-PD QWIP, the noise is increased by the square root of the gain $\sqrt{g}$ and the detectivity D^* is reduced by this same factor. As shown in Fig. 3.18, the optimum quantum well period for this BTM QWIP is 20, and further increase of the period has little or no effect on D^*.

3.3.6 Blocking Barrier and Dark Current

Using a $450 \overset{\circ}{A}$ thick of $Al_{0.16}Ga_{0.84}As$ barrier layer (with barrier height of 120 meV) adjacent to the end of superlattice barrier can effectively block undesirable tunneling carriers.[47,48] The quantum wells and the blocking layer are sandwiched between the heavily doped GaAs contact layers. The blocking barrier layer was designed so that the top of the barrier is lower than the bottom of the first excited-state, but much higher than the top of quantum well ground-state to block the flow of electrons (dark current) from the ground-state to the collector contact layer. The idea of employing such a blocking layer in a quantum well IR detector was first appeared in the work by Coon et al..[39] The performance improvement by the blocking layer can be seen from the reduction of electron

transmission coefficient near the ground-state as shown in Fig.3.19. The dark current density can be calculated by using the expression[46]

$$J_d = \frac{4\pi q m^* k T}{h^3} \int_0^\infty |T_r|^2 ln \left[\frac{1 + e^{(E_F - E)/kT}}{1 + e^{(E_F - E - qV_b)/kT}} \right] dE \qquad (12)$$

where V_b is the bias voltage across one period of the superlattice barrier, E is the electron energy, E_F is the Fermi level and T_r is the transmission coefficient. The dark current for the BTM QWIPs shown in Fig.3.16 with a blocking barrier is estimated to be below 10^{-6} A for $V_b \leq 0.4$ V and at T = 83 K.

3.3.7 Waveguide Structure

Using a 2-D planar metal grating coupler can greatly enhance the intersubband absorption in a BTM QWIP under normal incident illumination. A further increase in the coupling quantum efficiency can be obtained by incorporating a waveguide cladding layer underneath the active region of the quantum well layers. This structure is particularly effective for application where the total number of quantum well periods is small.[49] In such a structure, the whole QWIP behaves as an optical waveguide, as shown in Fig.3.20. The waves diffracted by the grating are confined in the transverse direction and guided along the longitudinal direction to allow radiation passing through the quantum well stack several times. The waveguide is formed by adding an internal reflecting layer beneath the QWIP active region to reflect the unabsorbed radiation back into the quantum well stack. The cladding layer and the top cap layer are deposited on each side of the quantum well stack. Since the refractive index of AlAs is $n = 2.76$, itis an adequate choice for use as a cladding layer of the InGaAs BTM QWIP.

In this section we perform a numerical analysis of the GaAs/AlGaAs grown infrared waveguide by using multi-slab waveguide mode theory.[50] For simplicity, we neglect the radiation loss by the metal grating and treat the waveguide without grating on the top. As shown in Fig.3.21, the index profile of the waveguide is assumed to be invariant in the direction of propagation, $\hat{z}$, which can be written as

$$\epsilon(y, z) = \epsilon_0 n^2(y, z) \qquad (13)$$

where ϵ_0 is the permittivity of free space, and $n(y, z)$ is the refractive index profile. The electromagnetic field of the guided mode in the waveguide can be expressed as

$$\vec{E}(x, y, z) = \vec{E}^0(y, z) e^{-j\beta x}$$

$$\vec{H}(x, y, z) = \vec{H}^0(y, z) e^{-j\beta x}$$

where the time dependence $e^{j\omega t}$ was omitted and β is the propagating constant of the mode. Due to the planar geometry of the waveguide QWIP, the guided fields are confined only to one direction, say $\hat{z}$, and are independent of the direction, $\hat{y}$, thus

$$\frac{\partial \vec{E}^0(y,z)}{\partial y} = \frac{\partial \vec{H}^0(y,z)}{\partial y} = 0$$

Besides, the planar waveguide supports two kinds of guided modes: TE mode has zero longitudinal electric field ($E_z = 0$), and TM mode has zero longitudinal magnetic field ($H_z = 0$). The field solution of TE modes are readily obtained by the field of TM modes according to the concept of duality,

$$\vec{E} \longrightarrow \vec{H} \qquad \vec{H} \longrightarrow -\vec{E}$$

$$\epsilon \longrightarrow \mu \qquad \mu \longrightarrow \epsilon$$

However, only TM modes can cause intersubband absorption, and hence the following discussion is focused on TM modes only. First, we separate Maxwell equations into transversal component and longitudinal component as

$$\nabla_t \times \vec{E}^0(y,z) + j\omega\mu\vec{H}^0(y,z) = j\beta\hat{z} \times \vec{E}_t^0(y,z)$$

$$\nabla_t \times \vec{H}^0(y,z) - j\omega\epsilon\vec{E}^0(y,z) = j\beta\hat{z} \times \vec{H}_t^0(y,z)$$

There exists three field components H_y^0, E_z^0 and E_x^0 for the TM modes. After a comparison of components in three directions, the above two equations can be expressed in the following forms

$$x \quad : \qquad \frac{\partial H_y^0}{\partial z} = j\omega\epsilon E_x^0$$

$$y \quad : \qquad \frac{\partial E_x^0}{\partial z} + j\beta E_z^0 = j\omega\mu H_y^0$$

$$z \quad : \qquad \beta H_y^0 = \omega\epsilon E_z^0 \tag{14}$$

Setting $\mathcal{H} = H_y^0$ and $\mathcal{E} = \omega\epsilon_0\epsilon_r E_x^0$, we have

$$\frac{d\mathcal{H}}{dz} = j\mathcal{E}$$
$$\frac{d\mathcal{E}}{dz} = -j(\beta^2 - n^2 k_0^2)\mathcal{H}$$

where k_0 is free space wave number. Both $\mathcal{H}$ and $\mathcal{E}$ are scalar wave solutions and obey the transverse wave equation

$$\mathcal{H}''(z) = (\beta^2 - n^2 k_0^2)\mathcal{H}(z) \tag{15}$$

39

The general solution of $\mathcal{H}$ and $\mathcal{E}$ are given by

$$\begin{aligned}
\mathcal{H}(z) &= Ae^{j\gamma z} + Be^{-j\gamma z} \\
\mathcal{E}(z) &= \gamma Ae^{j\gamma z} - \gamma Be^{-j\gamma z}
\end{aligned} \tag{16}$$

where A and B are constant of z, and

$$\gamma^2 = n^2 k_0^2 - \beta^2 \tag{17}$$

For one film, three-layer planar waveguide, we can solve the wave equation by setting the initial condition

$$\mathcal{H}_0 = \mathcal{H}(0)$$

$$\mathcal{E}_0 = \mathcal{E}(0)$$

at $z = 0$ and taking $\mathcal{H}(z)$ and $\mathcal{E}(z)/\epsilon_r(z)$ as continuous quantities in the $\hat{z}$ direction, The result is a matrix expression given by

$$\begin{pmatrix} \mathcal{H} \\ \mathcal{E} \end{pmatrix} = M_1 \begin{pmatrix} \mathcal{H}_0 \\ \mathcal{E}_0 \end{pmatrix} \tag{18}$$

where

$$M_1 = \begin{pmatrix} \cos\gamma z & \frac{j\epsilon_r}{\gamma}\sin\gamma z \\ \frac{j\gamma}{\epsilon_r}\sin\gamma z & \cos\gamma z \end{pmatrix} \tag{19}$$

is the characteristic matrix. Extending this concept to m-layer waveguide with width d_i of each layer and

$$M_i = \begin{pmatrix} \cos\gamma_i d_i & \frac{j\epsilon_i}{\gamma_i}\sin\gamma_i d_i \\ \frac{j\gamma_i}{\epsilon_i}\sin\gamma_i d_i & \cos\gamma_i d_i \end{pmatrix} \tag{20}$$

of each characteristic matrix, where $i = 1, \ldots, m - 2$. The characteristic equation of the QWIP waveguide system can be obtained by

$$\begin{pmatrix} \mathcal{H} \\ \mathcal{E} \end{pmatrix} = M_{m-2}|_{d_{m-2}} \cdots \cdot M_1|_{d_1} \begin{pmatrix} \mathcal{H}_0 \\ \mathcal{E}_0 \end{pmatrix}$$

For a guided mode, the electromagnetic fields in the substrate layer are evanescent wave and have the form

$$\mathcal{H}_s(z) = Ae^{\alpha_s z}$$

$$\mathcal{E}_s(z) = -j\alpha_s Ae^{\alpha_s z}$$

Similarly, the electromagnetic field in the cap layer are

$$\mathcal{H}_c(z) = Be^{-\alpha_c(z-d_{m-2})}$$

$$\mathcal{E}_c(z) = j\alpha_c Be^{-\alpha_c(z-d_{m-2})}$$

where α_s and α_c are real number. The final matrix expression is given by

$$\begin{pmatrix} B \\ j\alpha_c B \end{pmatrix} = \begin{pmatrix} m_{11} & m_{12} \\ m_{21} & m_{22} \end{pmatrix} \begin{pmatrix} A \\ -j\alpha_s A \end{pmatrix} \tag{21}$$

and the dispersion relation for a multilayer slab waveguide used to solve the propagating constant β is

$$j(\alpha_c m_{11} + \alpha_s m_{22}) = m_{21} - \alpha_s \alpha_c m_{12} \tag{22}$$

The active region of the BTM QWIP under analysis has a 20-period of quantum wells with an intersubband absorption peak at 10.5 μm wavelength as shown in Fig.3.17. The refractive index of GaAs, $Al_{0.38}Ga_{0.62}As$ and $Al_{0.16}Ga_{0.84}As$ are given by 3.25, 3.13 and 2.76, respectively.[52,53] Three parameters need to be determined are the thicknesses of the two ohmic contact layers and waveguide cladding layer. By adjusting the width of cap and bottom contact layers, the position of the maximum electric field intensity of the guided mode in the waveguide can be shifted. Figure 3.21 shows the electric field distribution of a 10 μm guided wave propagating in the waveguided BTM QWIP. From this figure, the cap layer must be much thicker than the bottom contact layer in order to draw the unbalanced field distribution to its maximum field intensity occuring in the QWIP active region. The combination of a 1.2 μm GaAs cap layer and a 0.5 μm bottom contact layer would yield a much better performance than that of the combination of a 0.5 μm cap layer and a 1.0 μm bottom contact layer. Thus, the optimum widths of contact layers can be determined.

The thickness of waveguide cladding layer is chosen such that the total QWIP layer thickness can be reduced significantly without inducing the excessive radiative mode leakage. For the present analysis, the cladding layer thickness is determined by the field intensity decreasing to 10 % of its maximum intensity at the interface of quantum well/AlAs cladding layer. This is a reasonable choice since it ensures a small residual waveguide loss within the QWIP absorption band. From Fig. 3.21, we have chosen a 4 μm thick of cladding layer for the BTM QWIP. Figure 3.22 shows the relative spectral detectivity (D^*) versus quantum well period for an InGaAs BTM QWIP with and without waveguide structure. From this figure, it is noted that a maximum detectivity for the BTM QWIP with waveguide structure was obtained for $N = 18$, while to obtain a maximum detectivity for the BTM QWIP without a waveguide structure requires a quantum well period exceeding 40.

In conclusion, we have performed a theoretical and experimental study on the effects of device structure and parameters on the performance of the InGaAs BTM QWIPs with three different quantum well periods. A BTM QWIP has the advantages over a BTC QWIP in that it can

effectively suppress the thermionic emission dark current as well as significantly increases the inter-subband absorption by using the enlarged quantum well and waveguide cladding layer underneath the active region of the quantum wells. Since the dark current is controlled mainly by the barrier height, by adding a selective blocking layer, the dark current can be further reduced. The doping concentration of the quantum well has little effect on the QWIP detectivity. On the other hand, the detectivity can be improved by using a large number of quantum wells in the QWIP. From the present study, an optimum quantum well period of 20 is obtained for the InGaAs BTM QWIP. Adding a δ μm AlAs cladding layer beneath the QWIP active region can greatly increase the coupling quantum efficiency. Increasing the width of the top contact layer to 1.2 μm and decreasing the bottom contact layer to 0.5 μm ensure a maximum absorption intensity of IR radiation traveling in the QWIP active region. Using the optimized parameters described in this section, the D^* of the InGaAs BTM QWIP can be increased by at least a factor of 2 over that of BTM QWIPs without the waveguide structure and parameter optimization.
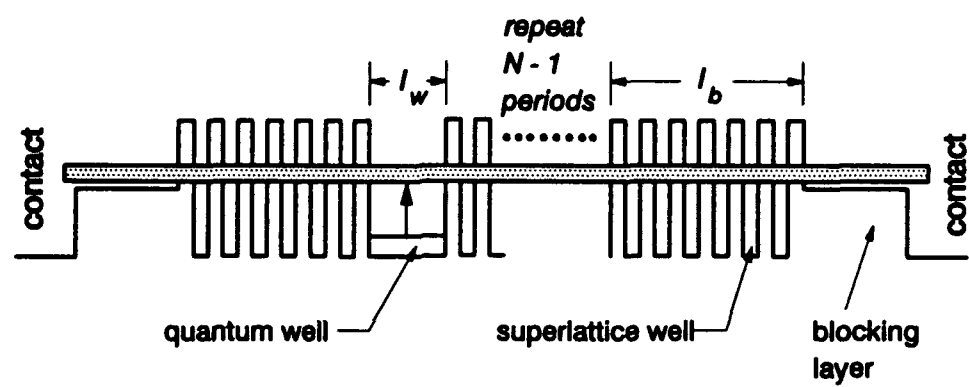
Figure 3.15 Energy band diagram of an N-period BTM QWIP with quantum well width l_w, superlattice barrier width l_b and the dark current blocking layers.
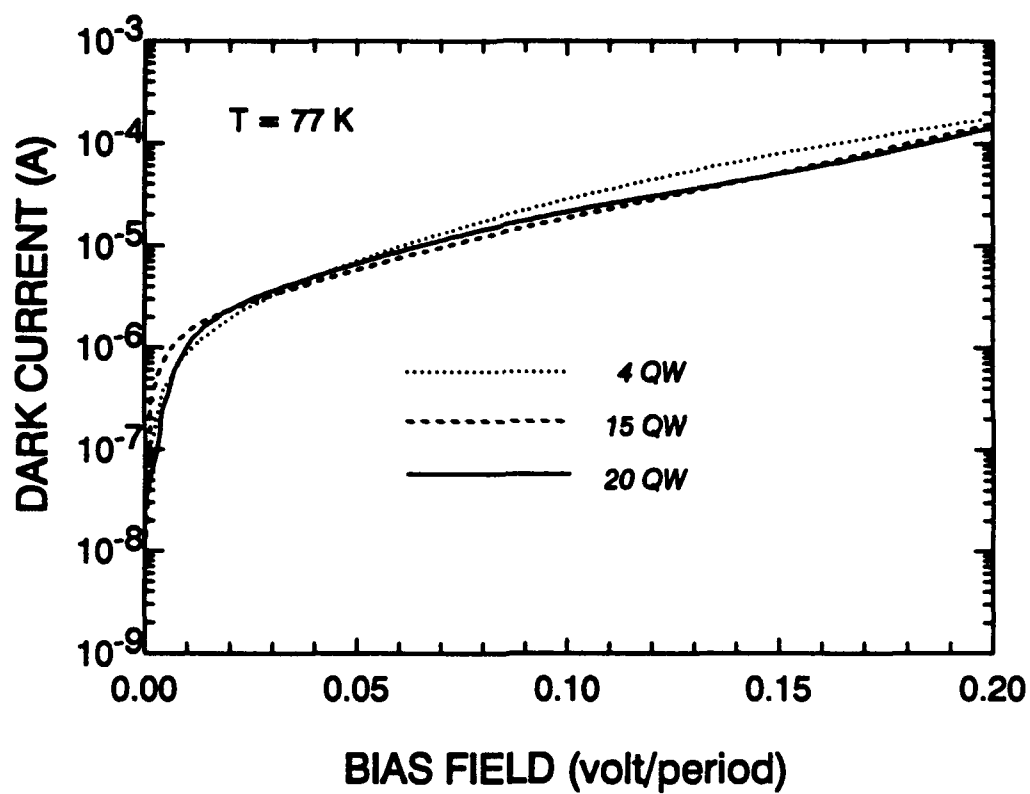
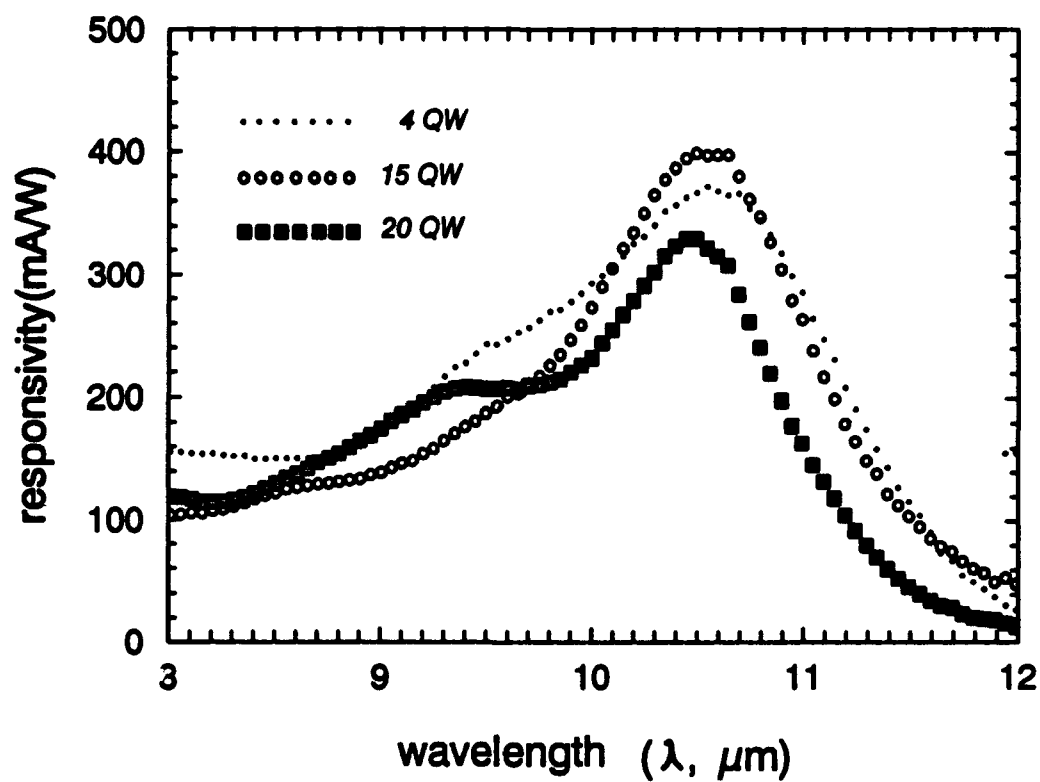**Figure 3.16** Dark current versus bias field for the 20PD, 15PD, and 4PD BTM QWIP measured at 77 K.

Figure 3.17 Spectral responsivity for the 20PD, 15PD, and 4PD BTM
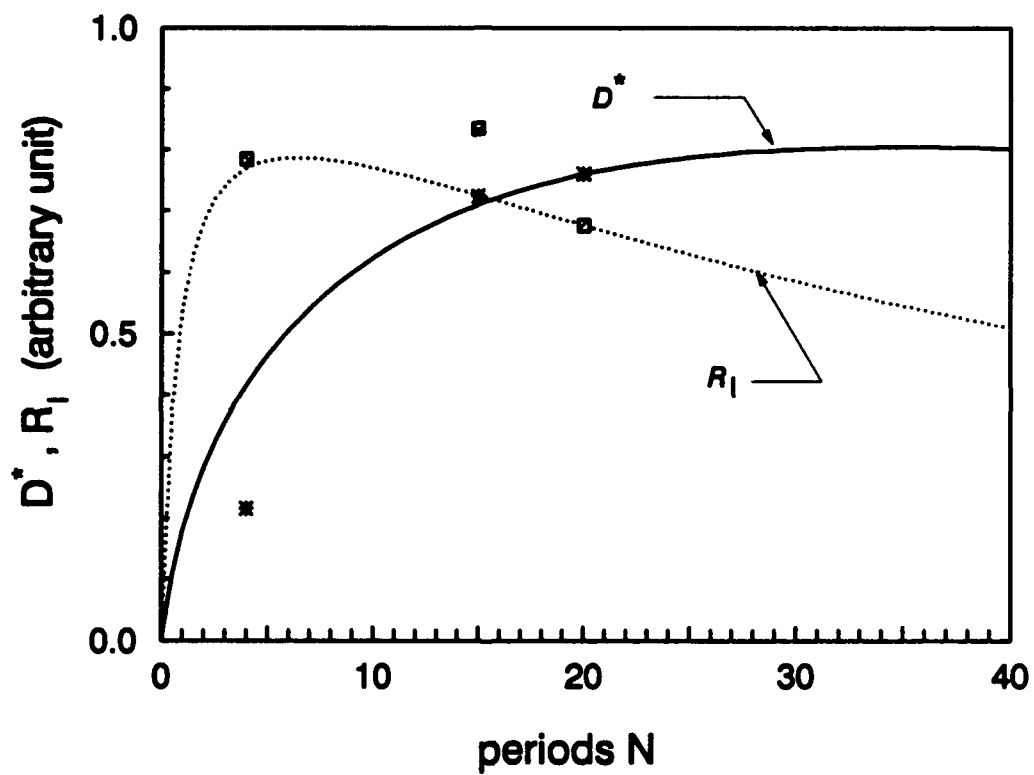QWIPs measured at $V_b = -0.1$ V/period.

Figure 3.18 A comparison of the calculated and measured relative responsivity R_I and detectivity D^* versus quantum well period N for the three BTM QWIPs without waveguide geometry. As shown in the figure, 20PD sample has the best fit.
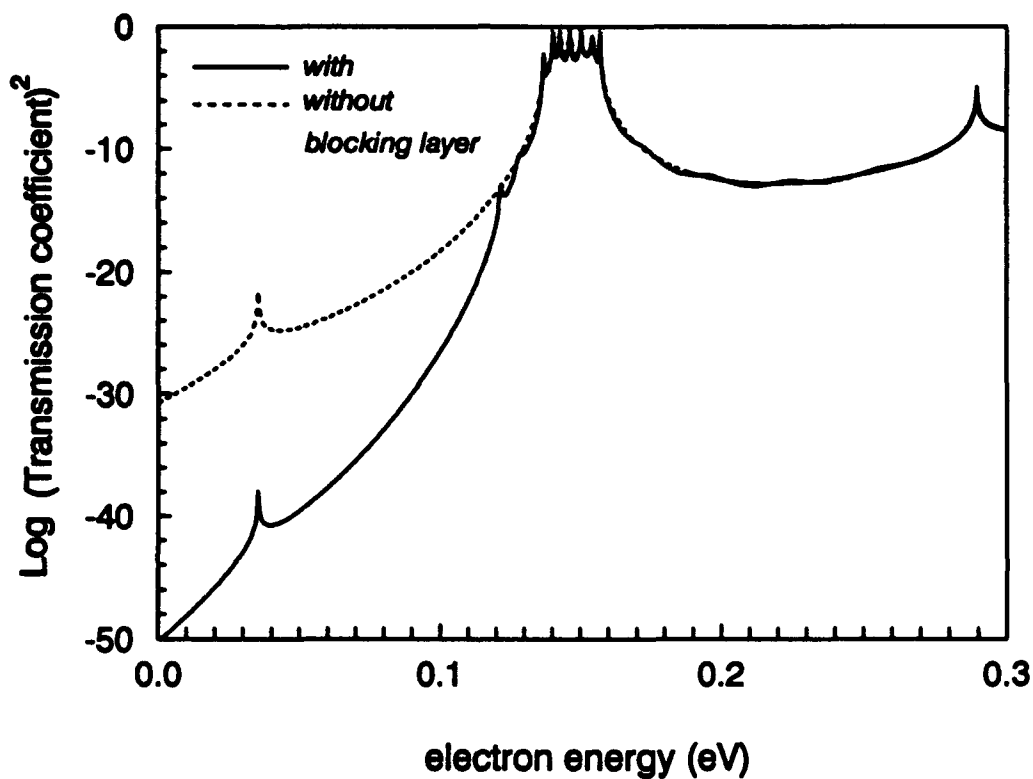
Figure 3.19 Calculated transmission coefficient T^*T versus the electron potential energy E (eV) through the superlattice barrier. The QWIP consists of 20 periods of doped $N_D = 7 \times 10^{17}$ cm^{-3} quantum wells of well width 93 $\mathring{A}$. The barrier layer on each side of the quantum well consists of 6 period undoped GaAs $(28\mathring{A})/$ Al$_{0.38}$Ga$_{0.62}$As (49 $\mathring{A}$) superlattice.
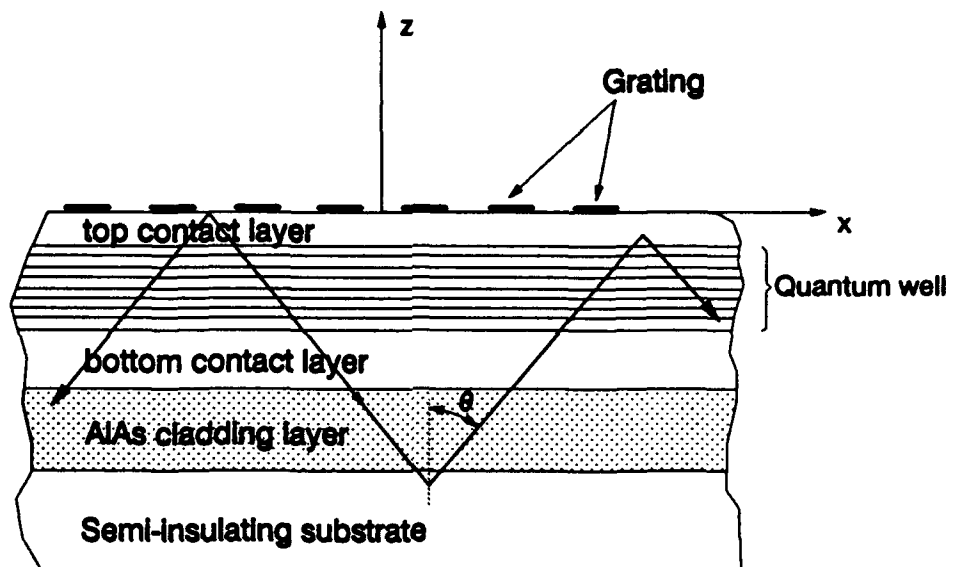
Figure 3.20 Side view of a waveguide geometry BTM QWIP showing the wave propagating in the structure.

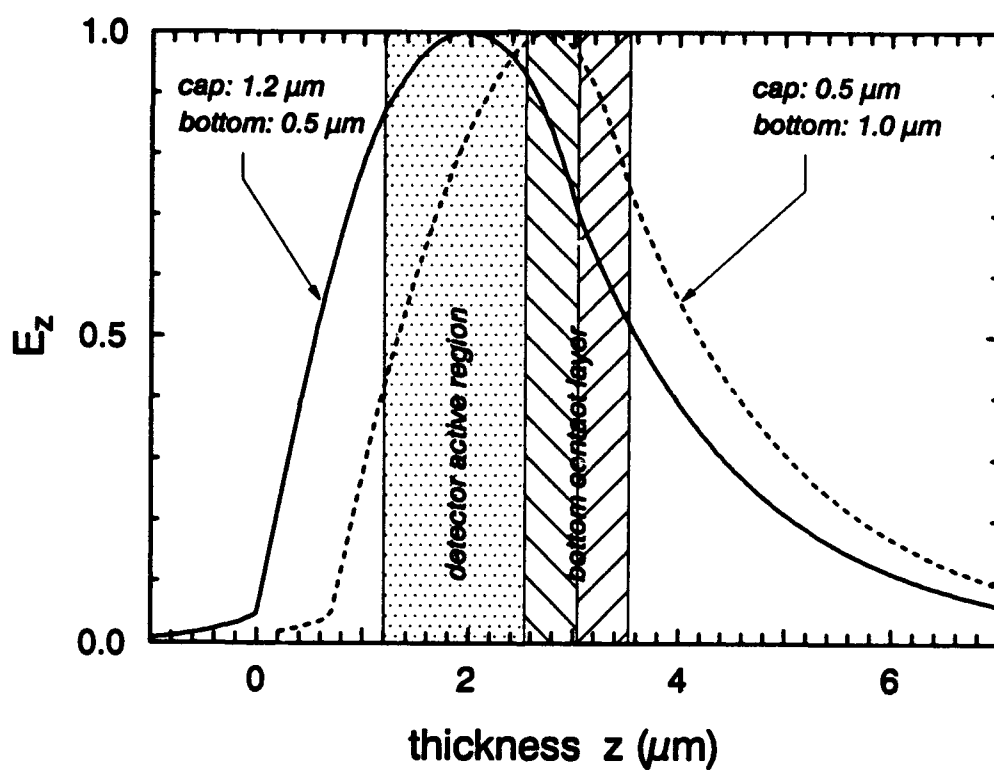**Figure 3.21** The electric field distribution of 10 μm guided wave versus the z axis for two sets of different widths of cap and bottom contact layers.
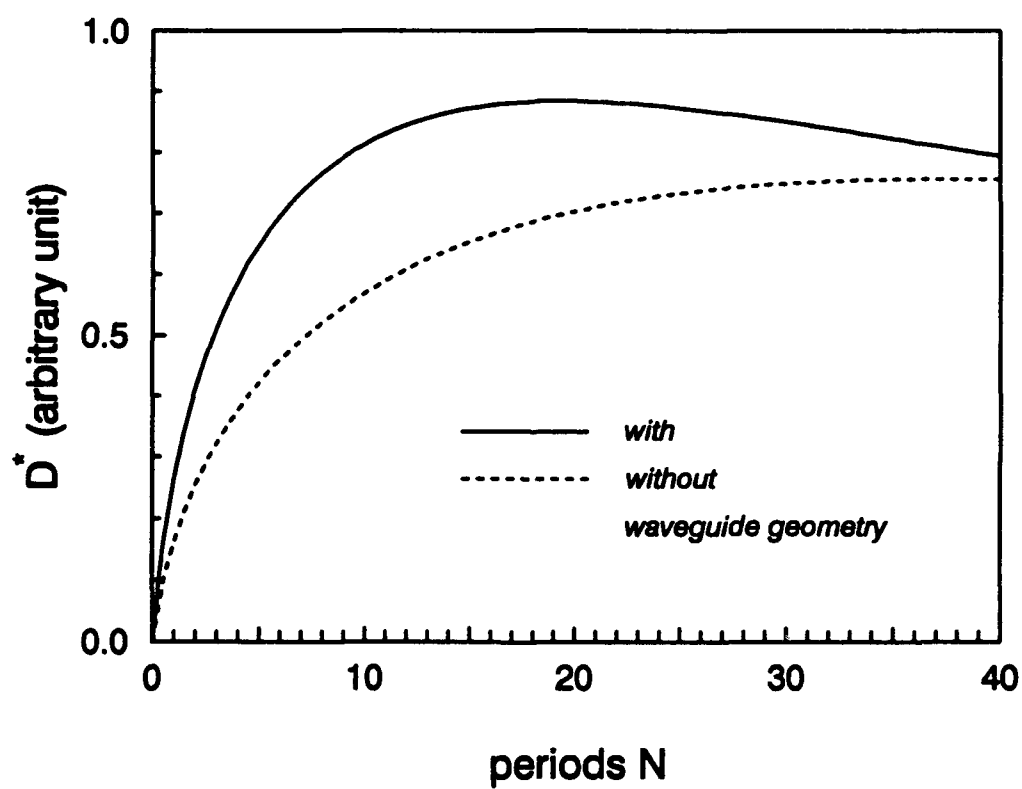
Figure 3.22 The theoretical prediction of detectivity D^* versus quantum well period N for the BTM QWIP with and without waveguide geometry of parameters given in Fig. 3.17.

3.4 References

1. B. F. Levine, J. Appl. Phys. **74**, R1-R81, (1993).

2. B. F. Levine, R. J. Malik, J. Walker, K. K. Choi, C. G. Bethea, D. A. Kleinman, and J. M. Vandenberg, Appl. Phys. Lett. **50**, 273 (1987).

3. L. S. Yu, S. S. Li, Appl. Phys. Lett. **59**, 1332 (1991).

4. G. Hasnain, B. F. Levine, C. G. Bethea, R. A. Logan, J. Walker, and R. J. Malik, Appl. Phys. Lett. **54**, 2515 (1989).

5. J. Y. Andersson and L. Lundqvist, J. Appl. Phys. **71**, 3600 (1992).

6. B. F. Levine, S. D. Gunapala, J. M. Kuo, S. S. Pei, and S. Hui, Appl. Phys. Lett. **59**, 1864 (1991).

7. B. F. Levine, S. D. Gunapala, J. M. Kuo, and S. Hui, Appl. Phys. Lett. **59**, 2864, (1991).

8. J. Katz, Y. Zhang, and W. I. Wang, Electron. Lett. **28**, 932 (1992).

9. W. S. Hobson, A. Zussman, B. F. Levine, and J. deJong, J. Appl. Phys.**71**, 3642 (1992).

10. Y. H. Wang, S. S. Li, J. Chu, and Pin Ho, Appl. Phys. Lett. to be published in Feb. issue, (1994).

11. E. O. Kane, Semiconductors and Semimetals, ed. R. K. Willardson and A. C. Bear, Vol. 1, 75 (1966).

12. F. H. Pollak, Semiconductors and Semimetals, ed. T. P. Pearsall, **32**, 17 (1990).

13. Y. C. Chang and R. B. James, Phys. Rev. **B-39**, 672 (1989); P. Man and D. S. Pan, Appl. Phys. Lett. **61**, 2799 (1992).

14. G. E. Bir and G. E. Pikus, "Symmetry and Strain-Induced Effects in Semiconductors", J. Wiley, New York (1974).

15. S. H. Pan, H. Shen, Z. Hang, F. H. Pollak, W. Zhuang, Q. Xu, A. P. Roth, R. A. Masut, C. Lacelle, and D. Morris, Phys. Rev. **B-38**, 3375 (1988).

16. K. Hirose, T. Mizutani, and K. Nishi, J. Crystal Growth, **81**, 130 (1987).

17. H. C. Liu, Z. R. Wasilewski, and M. Buchanan, Appl. Phys. Lett. **63**, 761 (1993).

18. Y. H. Wang, S. S. Li, and Pin Ho, Appl. Phys. Lett. **62**, 621 (1993).

19. J. S. Smith, L. C. Chiu, S. Margalit, A. Yariv, and A. Y. Cho, J. Vac. Sci. Technol. **B 1**, 376 (1983).

20. B. F. Levine, K. K. Choi, C. G. Bethea, J. Walker, and R. J. Malik, Appl. Phys. Lett. **50**, 1092 (1987).

21. L. S. Yu, Y. H. Wang, and S. S. Li, Appl. Phys. Lett. **60**, 992 (1992).

22. B. F. Levine, G. Hasnain, C. G. Bethea, N. Chand, Appl. Phys. Lett. **54**, 2704 (1989).

23. C. G. Bethea, B. F. Levine, V. O. Shen, R. R. Abbott, and S. J. Hsieh, IEEE Trans. **ED-38**, 1118 (1991).

24. C. G. Bethea, B. F. Levine, M. T. Asom, R. E. Leibengnth, J. W. Stayt, K. G. Glogovsky, R. A. Morgan, J. D. Blackwell, and W. J. Parrish, IEEE Trans. **ED-40**, 1957 (1993).

25. A. Köck, E. Gornik, G. Abstreiter, G. Böhm, M. Walther, and G. Weimann, Appl. Phys. Lett. **60**, 2011 (1992).

26. I. Gravé, A. Shakouri, N. Kuze, and A. Yariv, Appl. Phys. Lett. **60**, 2362 (1992).

27. K. Kheng, M. Ramsteiner, H. Schneider, J. D. Ralston, F. Fuchs, and P. Koidl, Appl. Phys. Lett. **61**, 666 (1992).

28. K. L. Tsai, K. H. Chang, C. P. Lee, K. F. Huang, J. S. Tsang, and H. R. Chen, Appl. Phys. Lett. **62**, 3504 (1993).

29. A. Kastalsky, T. Duffield, S. J. Allen, and J. Harbison, Appl. Phys. Lett. **52**, 1320 (1988).

30. B. F. Levine, S. D. Gunapala, and R. F. Kopf, Appl. Phys. Lett. **58**, 1551 (1991).

31. C. S. Wu, C. P. Wen, R. N. Sato, M. Hu, C. W. Tu, J. Zhang, L. D. Flesner, L. Pham, and P. S. Nayer, IEEE Trans. **ED-39**, 234 (1992).

32. Y. H. Wang and S. S. Li, P. Ho, Appl. Phys. Lett. **62**, 93 (1993).

33. Y. H. Wang and S. S. Li, P. Ho, Appl. Phys. Lett. **62**, 621 (1993).

34. H. Schneider, P. Koidl, F. Fuchs, B. Dischler, K. Schwarz, and J. D. Ralston, Semicond. Sci. Technol. **6**, C120 (1991).

35. H. Schneider, E. C. Larkins, J. D. Ralston, K. Schwarz, F. Fuchs, and P. Koidl, Appl. Phys. Lett. **63**, 782 (1993).

36. Y. C. Wang and S. S. Li, J. Appl. Phys. **75**, 582 (1994).

37. G. Hasnain, B. F. Levine, C. G. Bethea, R. G. Abbott, and S. J. Hsieh,

38. J. W. Choe, Byungsung O, K. M. S. V. Bandara, and D. D. Coon, Appl. Phys. Lett. **56**, 1679-1681 (1990).

39. D. D. Coon and R. P. G. Karunasiri, and L. Z. Liu, "Narrow band infrared detection in multiquantum well structures," *Appl. Phys. Lett.*, vol. 47, pp. 289-291, 1985.

40. B. F. Levine, C. G. Bethea, G. Hasnain, V. O. Shen, E. Pelve, R. R. Abbott, and S. J. Hsieh, *Appl. Phys. Lett.*, vol. 56, pp. 851-853, 1990.

41. B. F. Levine, "Quantum well infrared photodetectors," *J. Appl. Phys.*, vol. 74, pp. R33, 1993.

42. S. G. Gunapala, B. F. Levine, L. Pfeiffer, and K. West, *J. Appl. Phys.*, vol. 69, pp. 6517-6520, 1991.

43. A. Rose, *Concepts in Photoconductivity and Allied Problems* , Interscience, New York, 1963.

44. G. Hasnain, B. F. Levine, S. Gunapala, and Naresh Chand, *Appl. Phys. lett.*, vol. 57, pp. 608-610, (1990).

45. A. G. Steele, H. C. Liu, M. Buchanan, and Z. R. Wasilewski, *J. Appl. Phys.*, vol. 72, pp. 1062-1-64, 1992.

46. S. S. Li, M. Y. Chuang and L. S. Yu, *Semicond. Sci. Technol.*, vol. 8, pp. 406-411, 1993.

47. A. Kastalsky, T. Duffield, S. J. Allen, and J. Harbison,*Appl. Phys. Lett.*, vol. 52, 1320-1322, (1988).

48. C. S. Wu, C. P. Wen, R. N. Sato, M. Hu, C. W. Tu, J. Zhang, L. D. Flesner, Le Pham, and D. S. Nayer, *IEEE Trans. Electron. Devices*, vol. ED-39, 234-241, 1992.

49. G. Hasnain, B. F. Levine, S. Gunapala, and Nareah Chand, Appl. Phys. Lett., vol.57, pp.608-610 (1990).

50. T. Taimir, editor, *Guided Wave Optoelectronics,* (Springer-Verlag Berlin Heidelberg, New York, 1988), pp. 43.

51. M. A. Afromowitz, "Refractive index of $Ga_{1-x}Al_xAs$," *Solid State Commun.*, vol. 15, pp. 59-63, 1974.

52. J. Zorootchi and J. K. Butler,"Refractive index of n-type gallium arsenide," *J. Appl. Phys.*, vol. 44, pp. 3697-3699, 1973.